PWA FR-2596
20 NOVEMBER 1967

A STUDY OF THE SUPPRESSION OF COMBUSTION OSCILLATIONS WITH MECHANICAL DAMPING DEVICES

1 JULY 1966 TO 30 SEPTEMBER 1967

FINAL REPORT

PREPARED UNDER
CONTRACT NAS8-11038
FOR NASA - MSFC

Pratt & Whitney Aircraft DIVISION OF UNITED AIRCRAFT CORPORATION
FLORIDA RESEARCH AND DEVELOPMENT CENTER

PWA FR-2596
20 NOVEMBER 1967

A STUDY OF THE SUPPRESSION OF COMBUSTION OSCILLATIONS WITH MECHANICAL DAMPING DEVICES

1 JULY 1966 TO 30 SEPTEMBER 1967

FINAL REPORT

PREPARED UNDER
CONTRACT NAS8-11038
FOR NASA - MSFC

Approved by: G. D. Garrison
G. D. Garrison
Program Manager

Pratt & Whitney Aircraft DIVISION OF UNITED AIRCRAFT CORPORATION
FLORIDA RESEARCH AND DEVELOPMENT CENTER

FOREWORD

This report describes the work performed during the period 1 July 1966 to 30 September 1967 under Contract NAS8-11038 for the NASA, Marshall Space Flight Center. The NASA Technical Monitor was Mr. C. R. Bailey and Dr. Uno Ingard of the Massachusetts Institute of Technology served as technical consultant. The following personnel of Pratt & Whitney Aircraft contributed to the technical effort and preparation of the report: P.A. Marino, N. Bohn, P.L. Russell, A.C. Schnell, and G.L. Parsons. The Pratt & Whitney Aircraft Program Manager was Mr. G. D. Garrison.

ABSTRACT

The objectives of work conducted during the period 1 July 1966 to 30 September 1967 were: to determine the effects on liner absorption of simultaneous gas flows through and past the apertures, to investigate methods of improving the bandwidth characteristics of absorbing liners, and to determine the effects on absorption of differences in gas properties between the liner apertures and the combustion chamber. An impedance tube modified with flow ducts was used to measure the increase in liner acoustic resistance with flow; correlations of data with both flow velocity and Mach number are presented. Six different liner assemblies were evaluated in the bandwidth experiments. Theoretical analyses were made of the two assemblies that produced the greatest bandwidth improvement. A pressure-phase impedance measuring device was used in the gas property experiments; from the results it was concluded that the effects on sound intensity of a change in the medium through which a sound wave must travel can be predicted from one-dimensional theory. In addition, a standard impedance tube driven by a high-intensity electropneumatic transducer was used to measure the acoustic resistance of Helmholtz-type resonator arrays at incident sound pressure levels in the nonlinear regime. A simple correlation of the nonlinear resistance factor with sound pressure was obtained.

CONTENTS

CONTENTS (Continued)

ILLUSTRATIONS

ILLUSTRATIONS (Continued)

ILLUSTRATIONS (Continued)

NOMENCLATURE

Symbol	Description
A	Area
c	Sonic velocity
C_A, C	Acoustic capacitance
C_o	Hydraulic discharge coefficient
d, D	Aperture diameter
E_o, E	Electromotive force
f	Frequency
f_o	Resonant frequency
g	Gravitational constant
I	Sound intensity
J	Current
k	Wave length constant = ω/c
ℓ_{eff}	Effective aperture length
L	Backing distance
L_A, L_1, L_2	Acoustic inertance
M_p	Mach number of flow past apertures
M_t	Mach number of flow through apertures
P	Pressure
P_i	Incident pressure
P_r	Reflected pressure
P_t	Transmitted pressure
P_1	Total pressure in front of sample
P_2	Pressure in cavity
ΔP	Differential pressure
R	Resistance
SPL	Sound pressure level
s	Particle displacement
t, T	Liner thickness or sample thickness
u	Particle velocity
V	Volume
V_p	Velocity of flow past apertures
V_t	Velocity of flow through apertures

NOMENCLATURE (Continued)

Symbol	Description
$\Delta_n \ell/d$	Nonlinear resistance term
X	Acoustic reactance
X_L	Acoustic reactance with inductance only
X_c	Acoustic reactance with capacitance only
Y_1	Compressible gas flow factor
Z	Impedance
Z_{eq}	Equivalent impedance
α	Absorption coefficient
β	Ratio of diameters
θ	Specific acoustic resistance
θ_o	Specific acoustic resistance with no flow
θ_v	Specific acoustic resistance with flow
μ	Viscosity
ρ	Density
σ	Open area ratio
ω	Angular frequency
$\dot{w}$	Mass flow rate
ϕ	Phase angle
ψ	Constant = $\rho c/g$

SECTION I
INTRODUCTION

Absorbing liners, consisting of an array of Helmholtz resonators, have been used for many years at Pratt & Whitney Aircraft to eliminate combustion instability in airbreathing engines. The resulting experience suggested the basis for a similar approach to the solution of instability problems in rocket engines. With this overall objective, work was initiated in June 1963 under Contract NAS8-11038.

Throughout the first year, the program was divided into two major tasks (Reference 1)*. The first task required a complete and comprehensive survey of various mechanical damping devices that are used in rocket engine combustion chambers and airbreathing combustors. The second task involved an analytical study of the most promising damping devices that were found. The goals of the analytical study were (1) to formulate basic fundamentals of damping device design; (2) to devise installation schemes for suppressing the transverse, and possibly the longitudinal, modes of combustion instability; and (3) to formulate an experimental program necessary to support the analytical effort.

The literature survey revealed approximately 875 references concerning combustion oscillations of which approximately 60 were determined to be applicable to the mechanical damping of oscillations. All references included in the survey were compiled and published in a KWIC index. The most promising devices were injector baffles (reflecting devices) and absorbing or "screech" liners (absorbing devices).

An analysis of injector baffles and absorbing chamber liners was then conducted. A parametric analysis of an absorbing chamber liner was completed using techniques that were developed for turbojet afterburner liner design. The effects of gas media flow on absorbing liner performance were determined within the limitations imposed by the applicability of existing data. In addition, the heat transfer, stress, and weight problems, which are associated with the installation of an absorbing liner in a typical regeneratively cooled rocket chamber, were analyzed and an experimental program for obtaining the acoustic data needed to improve absorbing liner design technology was formulated.

*References are given in Section VIII.

At the completion of the first year of effort, Contract NAS8-11038 was amended to enlarge its scope and to increase the period of performance. The objectives of the amendment were (1) to establish experimentally the effectiveness of sound absorbers in suppressing combustion oscillations in rocket chambers; (2) to investigate qualitatively the performance of resonators; (3) to design long leadtime items needed in a cold flow acoustics test program; and (4) to devise methods of cooling sound absorbers in rocket engine combustion chambers. To achieve these objectives, the work described in the following paragraphs was accomplished (Reference 2).

Three acoustical absorbers were built and tested in a 10-in. diameter, LO_2/LH_2 combustion chamber. Results of these tests demonstrated the amount of absorption and the location of absorbing surfaces that are necessary to prevent combustion instability in the chamber.

To qualitatively study the performance of sound absorbers, a water table (or ripple tank) was designed and fabricated. The water table was selected for this purpose because the motion of waves on the surface of shallow water is analogous to the motion of acoustic waves in a gaseous medium.

The experimental program formulated as part of the first year's effort would require an apparatus that is capable of measuring the acoustic impedance of resonators that are subjected to high velocity gas flow and high intensity sound; however, the generation of sound pressure levels over 165 db* is a difficult problem. Therefore, the use of a bistable fluid oscillator as a high-intensity sound generator was experimentally explored. Results indicated that a substantial development effort would have to be expended to extend the sound pressure level obtained in preliminary tests to the required values (i.e., higher than 170 db). The recent availability of commercial high-intensity sound generators has rendered impractical further development of the fluid oscillator for this purpose.

*In this report all pressures expressed in decibels (db) are based on a reference pressure of 0.0002 microbar.

In addition, the cooling requirements of sound absorbers for use in rocket engine combustion chambers were analyzed, and suitable techniques were derived for convectively cooling absorbers. Considered in the analysis were regenerative cycles using four different propellant combinations at two chamber pressures.

At the completion of this phase of work, Contract NAS8-11038 was again amended to increase the scope of effort and (2) to lengthen the period of performance by 13 months, to July 1966. The objectives of the amendment (Phase II) were to expand and improve the acoustic damping theory, and to further develop the cooling techniques required for the use of acoustical absorbing devices in rocket engine combustion chambers. The results of these objectives are described in the following paragraphs (Reference 6).

An analytical program was conducted to extend and improve the mechanical damping theory used in the design of absorbing liners. The program included (1) the development of a theory for the design of nonresonant acoustic liners, (2) a study of the correlations of experimental data that could be used for predicting the nonlinear resistance of a resonator until more and precise data could be obtained, and (3) an investigation of the effects of incident sound pressure amplitude on liner design.

An uncooled liner test program was made to determine the amount of absorption required for suppression of combustion instability and to evaluate the effectiveness of liners made of ablative materials. Eight new absorbing liners were fabricated and 35 tests were conducted using two different combustion chambers. In addition, supplementary data were obtained on the effects of aperture flow and the temperature of the gas in the liner apertures and cavity.

Tests were made to evaluate experimentally the effects of flows and high sound pressure levels on the acoustical characteristics of absorbing liners.

Cooling methods for four different types of combustion chamber absorbing liners were analytically developed and analyzed. Also studied, in addition to film-cooled, transpiration-cooled, and convectively cooled

liners for preburner engine cycles, was a convectively cooled engine employing small rectangular slots as coolant passages.

At the completion of the Phase II work the contract was again modified to include the following tasks:

1. A determination of the effects on liner absorption of simultaneous gas flows through and past the apertures
2. An analysis to determine methods of improving the bandwidth characteristics of absorbing liners
3. An experimental determination of the effects on absorption of differences in gas properties between the liner apertures and the combustion chamber.

All work accomplished under the above three tasks is reported herein. In addition, an experiment conducted to determine the effects of high sound pressure levels on the specific acoustic resistance of absorbing liners is reported.

SECTION II
SUMMARY OF ACCOMPLISHMENTS

A summary of all work accomplished under the current phase of the program is given in the following paragraphs. All work was performed in the period from 1 July 1966 to 30 September 1967.

A. HIGH SOUND PRESSURE LEVEL EXPERIMENTS

For the design of acoustic liners, information is needed on the variation of acoustic resistance with sound pressure at levels above 160 db. When sound pressure levels are greater than 100 db, a nonlinear resistance to the sound wave must be considered in addition to the linear resistance. Because, at present, the nonlinear resistance of an array of resonators cannot be determined from theory, empirical correlations of experimental data must be used.

In the work reported herein, a standard ASTM-type impedance tube driven by a high-intensity electropneumatic sound generator was used, along with an improved data recording technique to measure the resistance of Helmholtz-type resonator arrays at incident sound pressure levels from 121 to 171 db. A simple correlation of the nonlinear resistance effects with sound pressure was obtained.

B. SIMULTANEOUS FLOW EXPERIMENT

An impedance tube modified with flow ducts was used to determine the effects of simultaneous flow on the acoustic resistance of liner samples. Tests were also conducted with flow past the apertures. In the simultaneous flow experiment, the velocity past the apertures was varied from 25 to 490 ft/sec and the flow-through velocity was varied from 100 to 400 ft/sec.

Results of the experiment showed that flow-past or flow-through causes the acoustic resistance to increase in proportion to the flow velocity. Flow-through was found to cause an increase in resistance seven times greater than that caused by flow-past of the same velocity. With simultaneous flows it was found that the effects of flow-past were negligible, for the resistance increased as though only flow-through were present. Correlations of data in the form of the increase in resistance with both flow velocity and Mach number are presented.

C. IMPROVEMENT OF ABSORPTION CHARACTERISTICS

In an effort to improve the absorption characteristics of acoustic liners, six different design concepts were experimentally evaluated. Analyses were made of the two designs that offered the greatest potential in achieving the objective.

Increasing aperture resistance with porous screens to improve absorption characteristics was attempted. Particular combinations of high open area resonators and low density porous backing plates proved to be the most effective. The result was an increased bandwidth performance accompanied by a reduction in absorption amplitude.

Nonresonant (porous) absorbing material with added conventional resonators were found to have a resonant frequency lower than theory would predict. No increased bandwidth performance was observed.

The dimpled resonator was evaluated, since the configuration offers a weight and space saving advantage in resonator array design. No improvement in the bandwidth characteristics over that of the conventional Helmholtz resonator array was noted.

A sample with different cavity volumes, and thereby different resonant frequencies, was found to possess high absorption coefficients that were independent of frequency. A similar configuration consisting of two parallel arrays of resonators was also found to have excellent absorbing bandwidth characteristics. A basic working theory for the parallel design was established using an acoustic-electric analog. Equations for predicting total absorption and procedures to be followed for computing the resonant frequencies are presented.

The double resonator in series was shown to possess resonant properties similar to those of the parallel design. A working theory was also established from an acoustic-electric analog for the series double resonator. Equations are presented for calculating total absorption and a procedure is given for computing resonant frequencies.

D. PROPERTY VARIATION EFFECTS

Rocket test data have shown that large temperature gradients exist between the gas in the combustion chamber and the gases in the apertures and cavities of absorbing liners. Experiments were therefore conducted to determine how the resulting variation in gas properties affected the liner absorbing characteristics.

The ASTM impedance tube was found to be unsuitable because of distortion in the standing wave pattern. To overcome the problem, an impedance apparatus was fabricated that eliminated the need to obtain data from a standing wave. The impedance apparatus was designed for a frequency range of 500 to 7000 Hz.

Using the new impedance device the property gradient within a rocket chamber was simulated by generating, in air, a sound wave at one end of an open duct. A resonator assembly, through which ambient helium could slowly be metered, was installed at the opposite end of the duct. From the experimental results it was concluded that the effects on sound intensity of a change in the medium through which a sound wave must travel can be predicted from one-dimensional theory. In addition, it was shown that if the properties of the gas in the apertures and cavity of an absorbing liner operating in such an environment are known, the acoustic performance of the array can be predicted within the limits of the present theory.

E. ADDITIONAL WORK ACCOMPLISHED

Additional impedance tests were conducted with a resonator array of 5.4% open area ratio using both the standing-wave impedance tube and the pressure-phase apparatus. Comparisons of the data with theory indicated that the present theory is inadequate for frequencies greater than resonance in the frequency range above 2000 Hz. It is therefore recommended that additional research be conducted with the objective of improving the absorbing liner design theory in the high frequency, high SPL regime. Until the problem is resolved, absorber designs for frequencies greater than 2000 Hz should be tuned for operation below resonance.

SECTION III
MEASUREMENT OF ACOUSTIC RESISTANCE AT HIGH SOUND PRESSURE LEVELS

A. INTRODUCTION

The parameter used for rating the performance of absorbing liners is the absorption coefficient (α), which is defined as the ratio of energy absorbed by the liner to the energy of the incident pressure wave. The coefficient is calculated from

$$\alpha = 1 - \left(\frac{Z - 1}{Z + 1}\right)^2 \qquad \text{(III-1)}$$

where Z is the specific acoustic impedance of the liner assembly. The acoustic impedance, defined as the ratio of incident pressure to the particle volume velocity, can be calculated from

$$Z = \theta + iX \qquad \text{(III-2)}$$

where θ is the specific acoustic resistance of the liner caused by the presence of the facing material (and apertures) and X is the specific reactance of the liner assembly, i.e., the liner facing and backing cavity. For a Helmholtz-type resonator, the reactance is composed of capacitance and inertance effects in the following manner:

$$X = \omega L_A - 1/\omega C_A = \frac{2\pi f_o \ell_{eff}}{c\sigma}\left(\frac{f}{f_o} - \frac{f_o}{f}\right) \qquad \text{(III-3)}$$

where ω is the angular frequency, L_A is the inertance due to the mass of the gas in the apertures and C_A is the capacitance due to the compressibility of the gas in the backing cavity.

The specific acoustic resistance is determined from

$$\theta = \frac{4}{\sigma\rho c}\sqrt{\frac{\mu\rho\omega}{2g}}\left(1 + t/d + \Delta_n\ell/d\right) \qquad \text{(III-4)}$$

In the above equation the terms 1 and t/d represent the viscous losses in the facing and neck of the aperture, while the $\Delta_n\ell/d$ term represents the additional losses encountered at high sound pressure levels. For high sound levels $\Delta_n\ell/d$ becomes the dominant term because as sound intensities approach 140 db,

changes in the circulation patterns and turbulence levels in the apertures of the liner take place. A nonlinear increase of resistance with sound pressure level results. The effects of high sound intensities on the components of impedance for a liner assembly are illustrated in figure III-1.

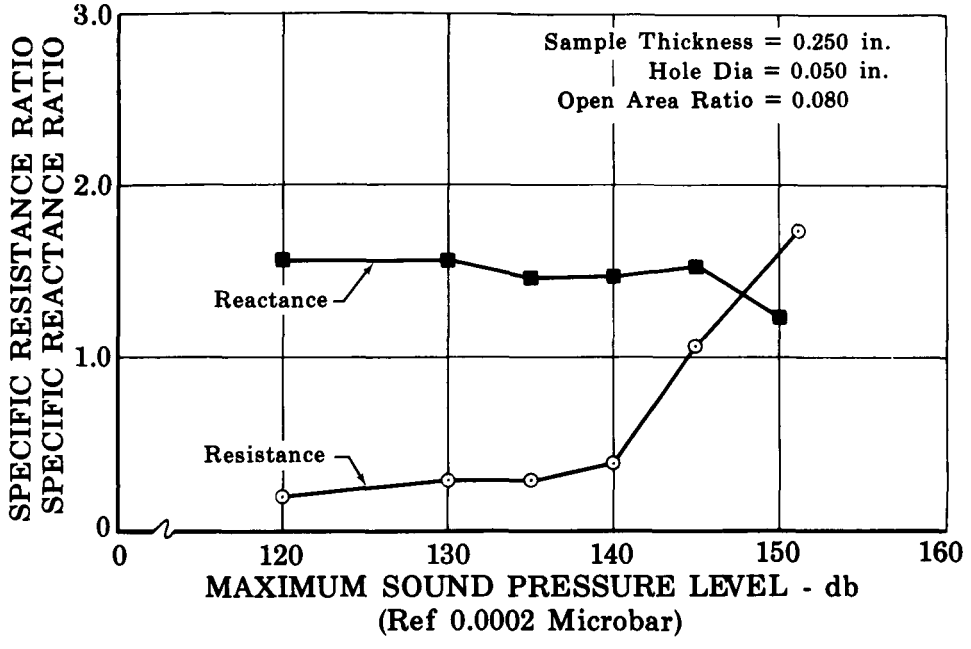

Figure III-1. Acoustic Reactance and Resistance Data vs Sound Pressure Level FD 23130

Because the resistance of a resonator array operating in the nonlinear regime can not yet be determined theoretically, empirical correlations of experimental data must be used (References 3 and 4). Unfortunately, the generation of high-intensity sound in a controlled experiment is a difficult problem. For the design of absorbing liners (arrays of resonators) only Blackman's data were known to be available (Reference 4); however, correlations based on these data may not be valid. As shown in figure III-2, the sample was badly scattered and, in addition, limited to sound pressure levels of 160 db or less.

The recent availability of commercial high-intensity sound generators has made possible an investigation to determine the nonlinear resistance of resonator arrays at incident sound pressure levels from 121 to 171 db. The experimental apparatus consisted of a standard (ASTM) impedance tube

with a refinement in the data recording process that led to a significant improvement in precision over that of the data published by Blackman.

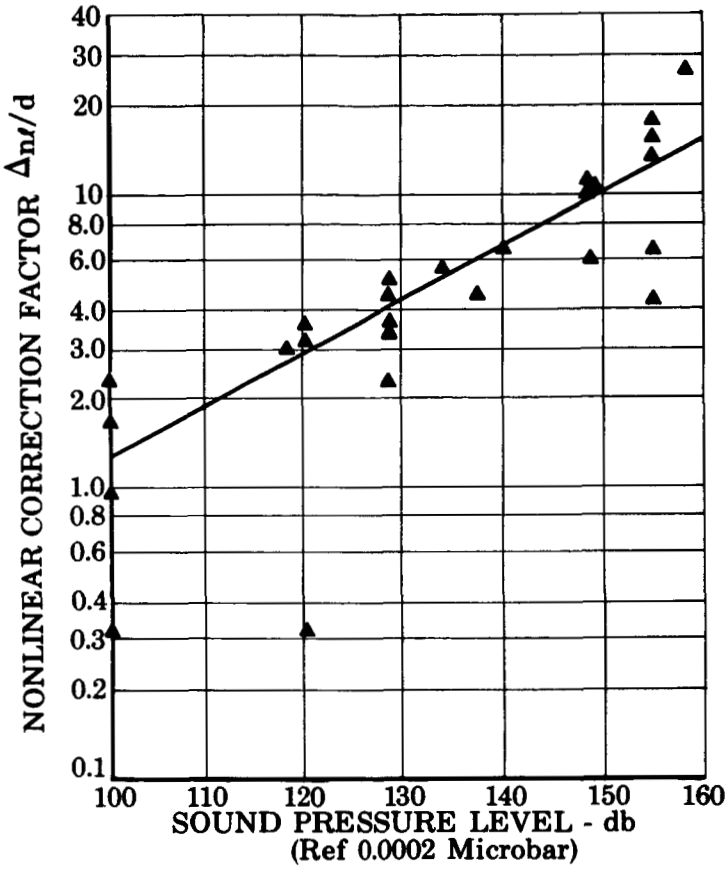

Figure III-2. Nonlinear Resistance vs Intensity Level, Blackman's Data FD 23131

B. METHOD OF TEST

The acoustic resistance of resonator samples was obtained using conventional impedance tube techniques. The tube was fabricated according to the standards set forth by the American Society for Testing Materials (Reference 5) for use in the frequency range of 400 to 2000 Hz. A Ling EPT-94-B air-modulating transducer was used as the source of high-intensity sound. The bleed tubes located in the exponential horn (figure III-3) permitted the gaseous nitrogen from the sound source to be vented to the atmosphere. To minimize the loss of sound energy, the tubes were of

quarter-wave length and therefore had to be replaced with a different set each time the test frequency was changed. An Altec microphone, type 2-BR-180, mounted on a calibrated probe tube* was used to determine the standing wave pattern in the tube; the signal was recorded on a strip chart. Also recorded on the chart was the distance from the sample traversed by the microphone probe. The distance was recorded by graphically displaying each revolution of the lead screw that drives the probe (figure III-4). The trace of the lead screw displacement has two frequencies because the strip chart was operated at a constant speed whereas the lead screw drive motor was operated at two different speeds (low speed in the vicinity of the minimum pressure point). The two traces could be used to determine the distance from the sample to the pressure minimums within ± 0.005 in. Three resonator array samples with circular apertures were used; each had a different geometrical configuration as described in table III-1.

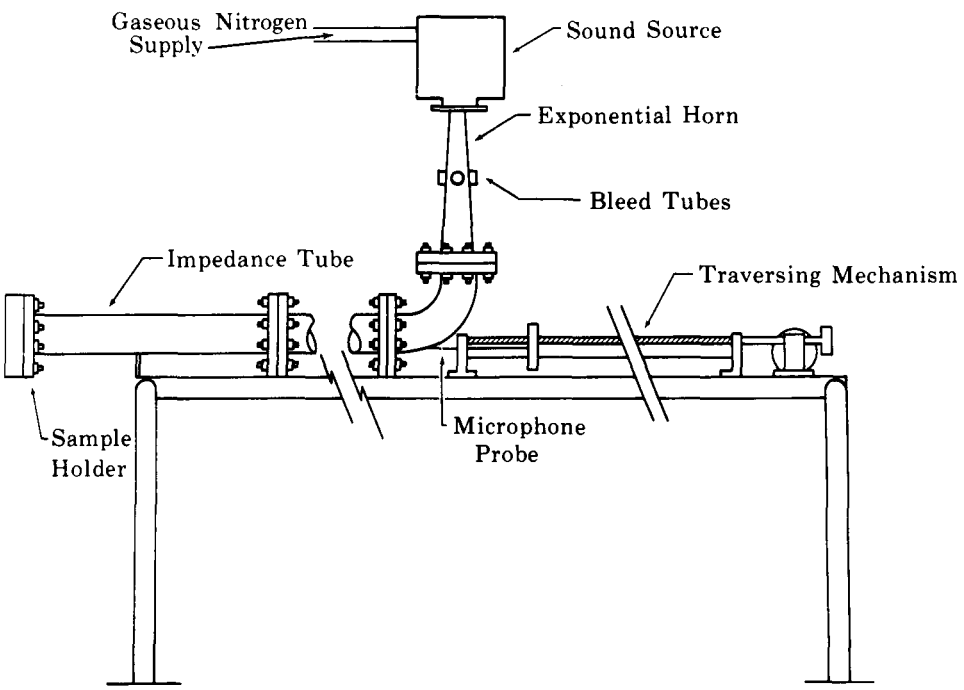

Figure III-3. Sketch of Impedance Tube FD 15556B

*Calibration of the probe tube is necessary to account for the sound attenuation caused by viscous and heat-conduction effects that occur in the probe tube.

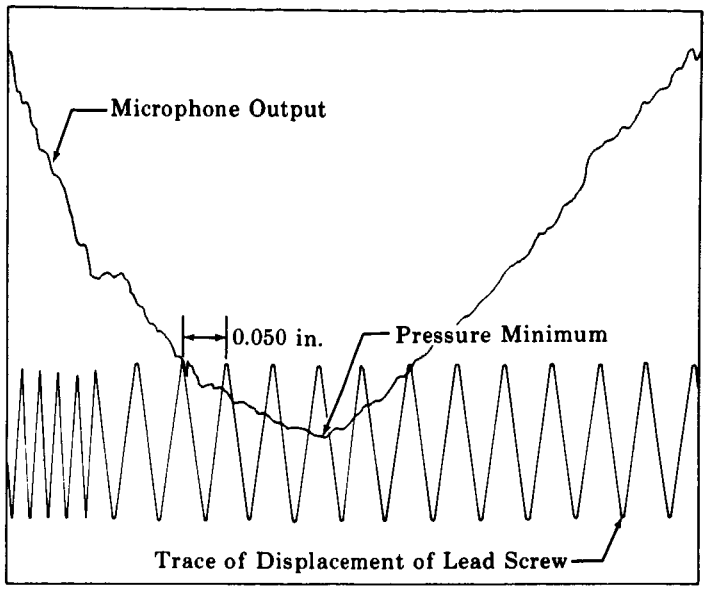

Figure III-4. Typical Impedance Tube Data Point, FD 18287

Table III-1. Description of Test Sample Geometry

Sample Thickness, in.	Aperture Diameter, in.	Open Area Ratio, %	Backing Distance, in.
0.250	0.050	10	0.50
0.250	0.050	5	0.50
0.250	0.078	3.06	0.50

C. RESULTS

For a particular resonator, the relationship between sound pressure and particle velocity in the aperture is given by

$$u = 2\pi fs = \left| \frac{2P_i}{\sigma\rho c \quad [(\theta + 1) + iX]} \right| \qquad \text{(III-5)}$$

An increase in particle velocity causes changes in the circulation patterns and turbulence levels in the apertures of the resonator, resulting in an increase of resistance. For sound levels greater than 100 db, the resistance is a nonlinear function of both particle velocity and sound pressure level.

In an attempt to determine the change in nonlinear resistance with high amplitude sound, the resistance was experimentally determined, and the nonlinear correction term, $\Delta_n \ell/d$, was computed using equation (III-4).

The $\Delta_n \ell/d$ term was then correlated with the pressure of the incident sound wave; the results are shown in figure III-5. It was found that the line shown in figure III-5 could be expressed by

$$\Delta_n \ell/d = 1.62 (P_i)^{0.98} \qquad \text{(III-6)}$$

an average data point deviation of less than 20%.

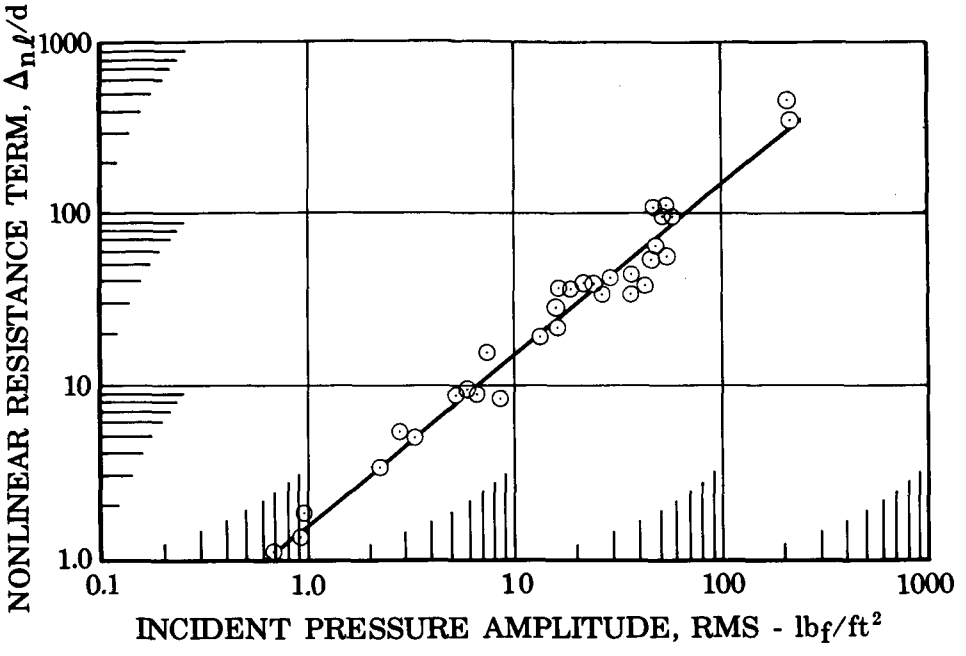

Figure III-5. Nonlinear Resistance Data FD 19156C

Comparison of the new data with the earlier results, figure III-6, shows that considerable differences exist. The new data do not agree with Ingard's results (Reference 3) probably because his experiments were conducted using only a single resonator, whereas the new data were obtained using multiple resonators. The facing configuration (and therefore the acoustic resistance) of an array of resonators is quite different from that of a single resonator, hence differences in the nonlinear resistance data from each should be expected. Note in figure III-6 that the slope of the line representing the P&WA data is approximately the same as that of the Ingard correlation. The agreement in slope suggests that the turbulence patterns that produce the nonlinear effects are similar for both single and multiple resonators, and only the absolute value of the term, for a particular sound level, is affected by the facing configuration.

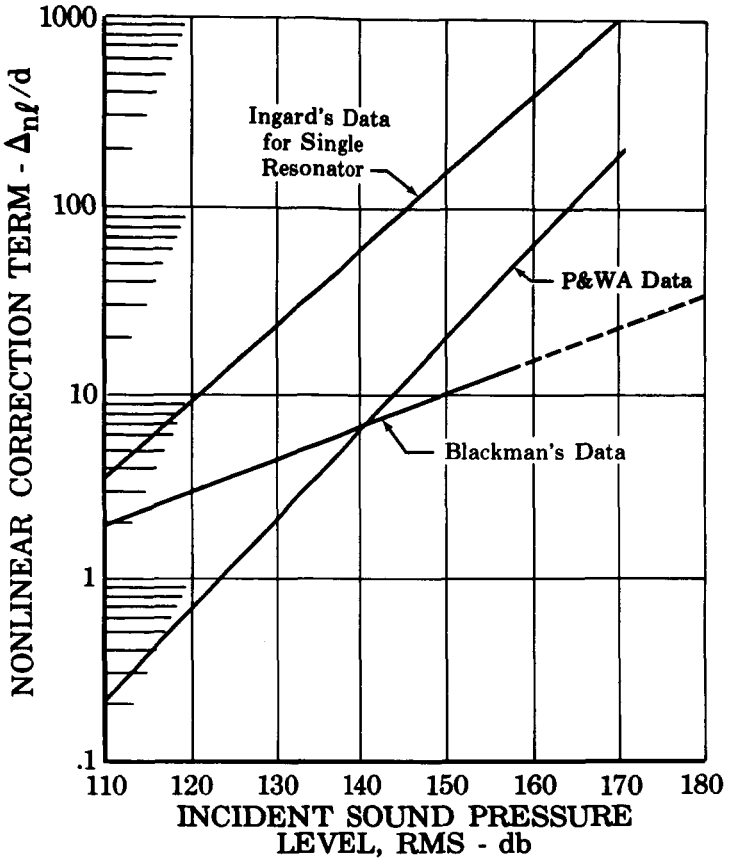

Figure III-6. Comparison of Nonlinear Correction Data FD 19155D

The reason for the difference between the new data and the earlier results of Blackman (Reference 4) is not as obvious. Because of the large scattering of the earlier data a high degree of correlation was not obtained, and the data scatter was taken as an indication that the nonlinear resistance is a complex function of many variables. However, the new results do not exhibit such data scatter, and consequently do not confirm the earlier conclusion on the origins of the nonlinearity. The primary differences in the experiments conducted by Blackman and those of the present work are in the thicknesses of the facing samples and in the method of taking data. Blackman used several thin (0.0625 in.) samples and obtained data only at the resonant frequency. In the later experiments, three 0.250-in. thick samples were used, and data were taken over a range of frequencies from 400 to 2000 Hz in increments of 400 Hz.

The possibility remains that the scatter in the earlier data was caused by extraneous variables that are unique to thin arrays of resonators at the resonant frequency.

D. CONCLUSIONS AND RECOMMENDATIONS

From the results of the above experiment it is concluded that the portion of acoustic resistance due to high incident sound pressures can be accurately measured and correlated with incident pressure in a form useful for absorbing liner design studies. However, as pointed out in References 6 and 10, the incident pressure amplitude must be assumed for input to the design procedure; an arbitrary value of 190 db has in the past been recommended for use with the Blackman data. An investigation was made of the effects of that recommendation on the absorbing liner design process using the new nonlinear resistance data. The absorption coefficients for three of the uncooled liners used in the Phase II test program, Reference 6, were recalculated. The resulting coefficients for all of the liners were found to be less than 2% and, furthermore, as shown in figure III-7, the curve of absorption coefficient versus open area ratio was found to be linear with open area ratio (i.e., the familiar bell-shape curve was not exhibited). Further analysis revealed that if equation (III-6) is extrapolated to 190 db, the resulting nonlinear correction to the specific acoustic resistance forces the resistance to be several orders of magnitude greater than the reactance, and the absorption coefficient becomes simply

$$\alpha \approx 4/\theta$$

Since the reactance terms are negligible, no bell-shape characteristics can be evident in the curve of absorption coefficient with open area ratio. Also, as is evident in equation III-4, the resistance is inversely proportional to σ, the open area ratio; therefore, for a constant incident pressure, the absorption coefficients will be directly proportional to σ.

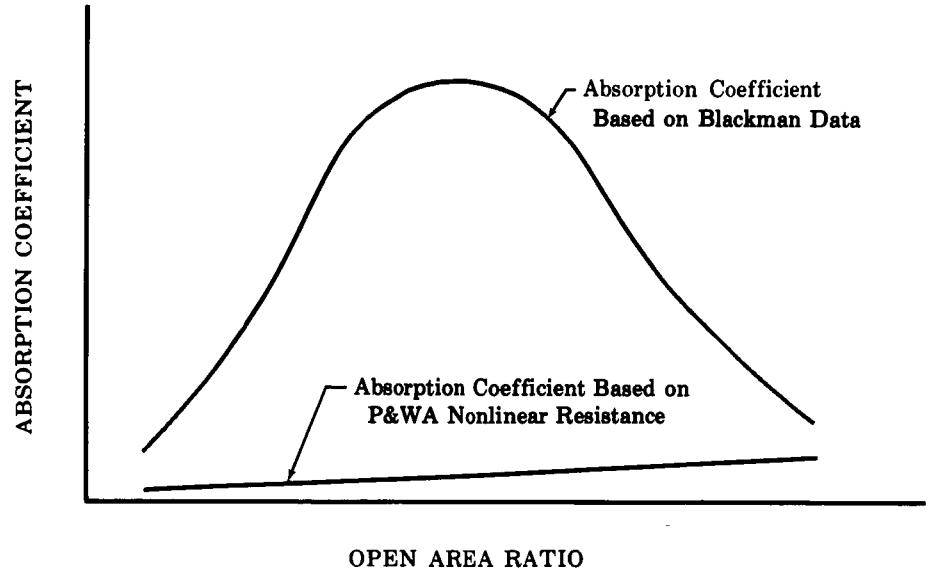

Figure III-7. Comparison of Design Theories With Assumed Incident Pressure of 190 db FD 15225B

The results of the test of liners with high open area ratios (also reported in Reference 6) indicated that the uncooled liners did exhibit resonant characteristics. It is therefore concluded that the assumption of 190 db for the incident pressure for use in equation (III-6) is much too high and the new nonlinear data correlation should not be extrapolated. Instead, an incident pressure of 171 db (150 lb_f/ft^2) or less must be assumed. In addition, the absorption coefficient of a particular design should be checked over a range of incident pressure levels as it is now done to investigate the frequency response characteristics of a liner.

The assumed incident pressure now constitutes the greatest uncertainity in the liner design procedure. It is recommended that additional research be conducted in an attempt to verify or improve the assumption.

SECTION IV
SIMULTANEOUS FLOW ANALYSIS

A. INTRODUCTION

An absorbing liner consists of a perforated cylindrical element that is concentric to, and separated from, the combustion chamber pressure shell by support rings. Absorbing liners must, in many cases, be designed for situations in which there is a net flow of gas through, as well as past, the resonator apertures (see figure IV-1). This condition (simultaneous flow) occurs in rocket engines that have small contraction ratios and/or tapered combustion chambers because the chamber pressure decreases rapidly along the liner axis.

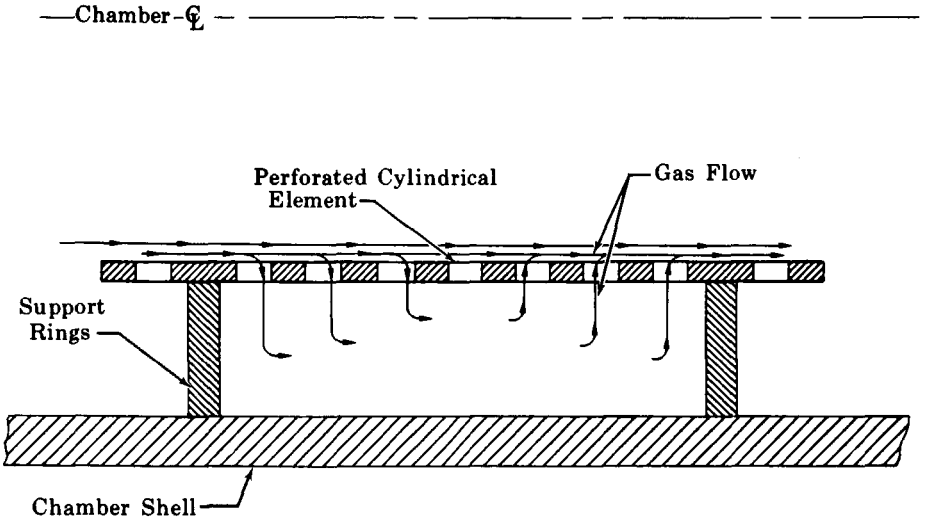

Figure IV-1. Absorbing Liner With Simultaneous Flow Conditions FD 23051

At present, no satisfactory theory is available for designing an absorbing liner that is subjected to simultaneous flows. Data from cold-flow tests were needed before a comprehensive theory could be developed;

therefore, a series of impedance tube tests was conducted to investigate the effect of simultaneous flow on the acoustic properties of absorbing liners.

In the previous year's effort, a series of impedance tube tests was conducted to investigate the effects of flow past the apertures on the acoustic properties of liners. In a second series of tests, the effects of flow through the apertures were determined experimentally. The results of both experiments are reported in Reference 6. The simultaneous flow experiment required the use of a more sophisticated flow instrumentation system than that used in the previous two experiments. The use of the new instrumentation significantly reduced the scatter in the data; therefore, the flow-past and the flow-through experiments were repeated, and the data were used to form more precise correlations of the acoustic resistance with flow than those reported in Reference 6.

B. TEST PROCEDURE

The first tests were conducted in an attempt to determine the effects of simultaneous flow on acoustic resistance; however, analysis of results showed a high degree of data scatter. Further study of the data revealed that the system for measuring flow velocities was inadequate and that the values used to represent flow conditions were possibly in error. Therefore, the following alterations to the impedance facility were made (refer to figure IV-2):

1. Pitot tubes were installed in place of the Kiel probe tubes. By using the pitot tube, the ratio of static-to-total pressure could be held constant, and thereby constant flow-past Mach numbers could be maintained. Also, the effect of compressible gas flow was taken into account.
2. A static pressure tap was located upstream of the sample. By measuring the static pressures upstream of the sample and in the duct, the drop in pressure across the apertures was known. From the following equation (Reference 7), the hydraulic discharge coefficient of the apertures could be calculated:

$$\dot{w} = C_o \, A \, Y_1 \sqrt{\frac{2g\rho \, \Delta P}{1 - \beta^4}}$$

The term, Y_1, takes into account the effect of compressible gas flow to the apertures.

3. Calibrated flow orifices were installed in both nitrogen supply lines (see figure IV-3). The orifice in the supply line to the driver sensed the flow passing through apertures when the bleed pipes were shut, allowing no flow to escape. Knowing the flow supplied to the sample apertures, and the hydraulic discharge coefficient, the flow velocity through the apertures could be calculated. Using data from the orifice in the duct supply line and the static pressure tap on the pitot tube, the average velocity past the apertures was determined.

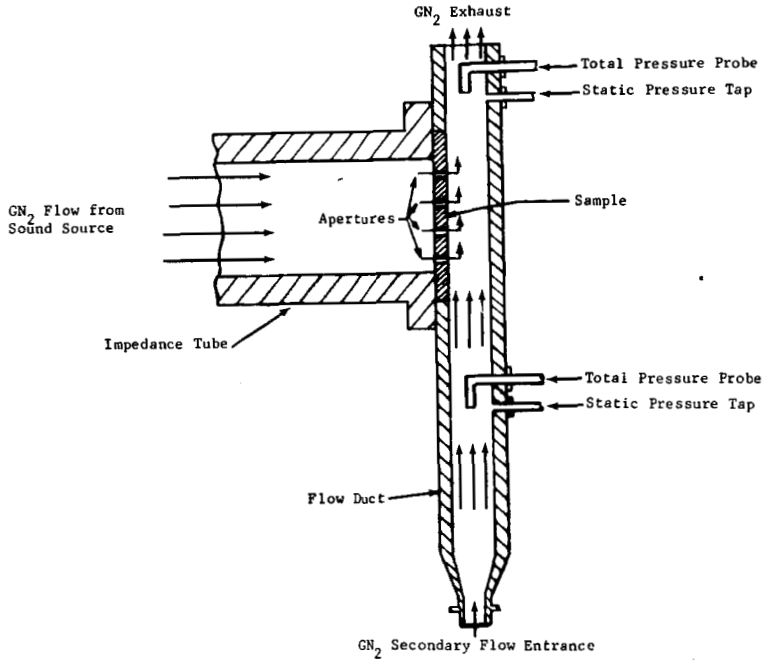

Figure IV-2. Simultaneous Flow Apparatus FD 20129

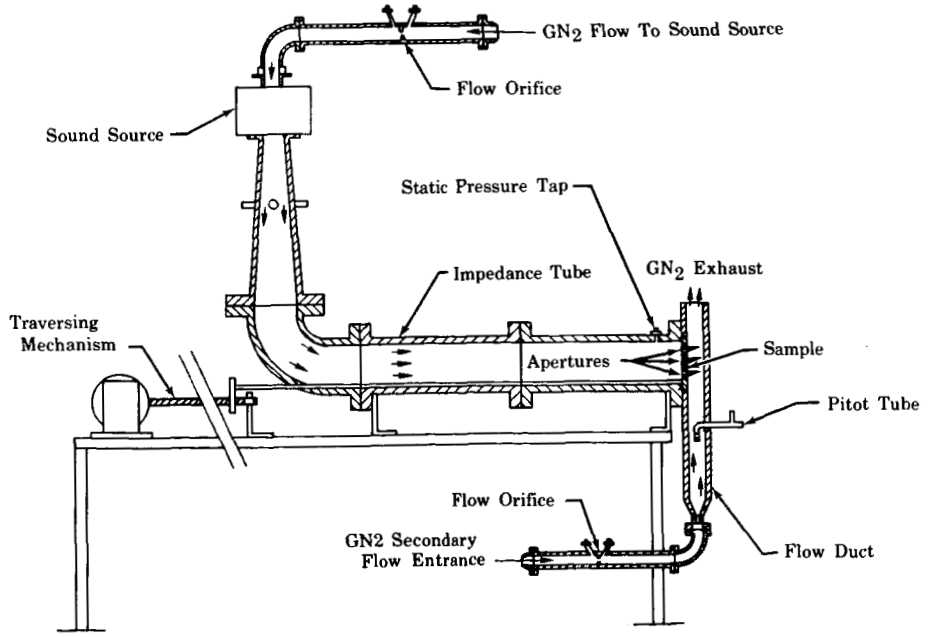

Figure IV-3. Simultaneous Flow Apparatus FD 21980

In addition, an experiment was performed to determine what effects the velocity gradient in the flow duct had on the measured velocity. Results indicated that the average velocity in the duct was 85% of the maximum velocity, which occurred in the center of the duct. Either the maximum or average velocity could be used in data correlations. It was arbitrarily decided that all correlations of data with flow-past would be based on the average velocity in the duct.

The flow-past and flow-through experiments were repeated in an attempt to improve the data precision over those reported in Reference 6. The effects of flow-past only on the resistance of the sample were first determined. Average velocities past the apertures were set at 0, 100, 200, 300, 400, 500, and 600 ft/sec. The effects of flow through the apertures on the resistance of the sample were then determined. Average velocities through the apertures were set at 200, 300, 400, 500, and 600 ft/sec.

Finally, the effects of simultaneous flow on the resistance of the sample were determined. The flow velocities past the apertures were set at seven different values: 33, 53, 75, 84, 98, 278, and 490 ft/sec. At each of these settings flow-through velocities were set at approximately 10, 25, 50, 100, 200, 300, and 400 ft/sec.

All flow tests were conducted using a sample having a nominal open area ratio of 10.8%, thickness of 0.250 in., and aperture diameter of 0.052 in. Results of initial tests indicated that changes in frequency had no significant effect on the change in acoustic resistance with flow; therefore all tests were made at one frequency (800 Hz). Throughout all of the flow experiments, a constant total sound pressure level of 160 db was maintained at the sample face.

C. RESULTS

Results of the flow-past and flow-through experiments are shown in figures IV-4 through IV-7, in which the ratio of the acoustic resistance with flow to that with no flow has been correlated with both the velocity and Mach number. The results show that when either type of flow is present the acoustic resistance of the sample varies in direct proportion to the velocities. From the differences in slopes between figures IV-4

PAGES IV-5 AND IV-6 ARE MISSING FROM THE ORIGINAL DOCUMENT.

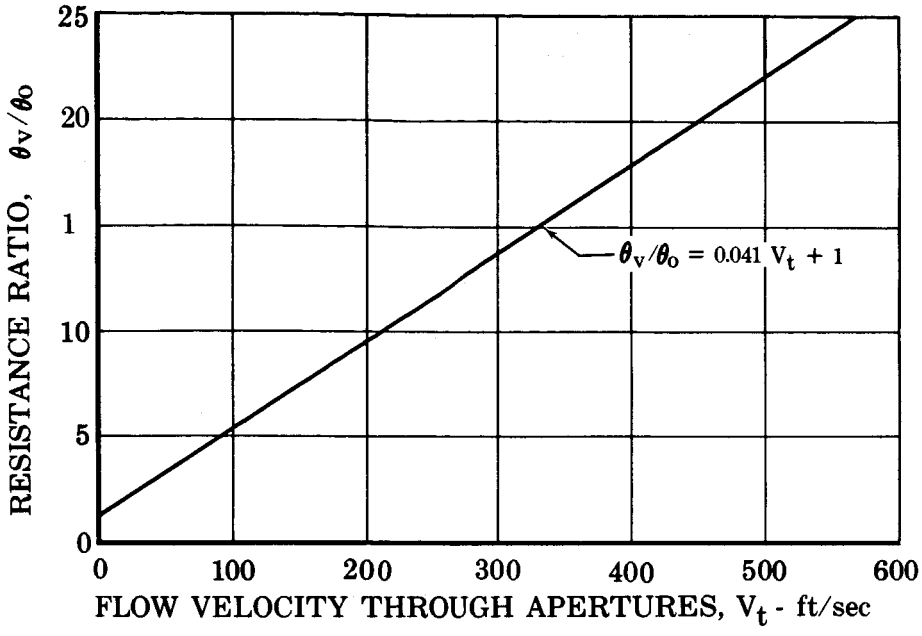

Figure IV-6. Resistance Ratio as a Function of Gas Velocity Through The Apertures

FD 21982A

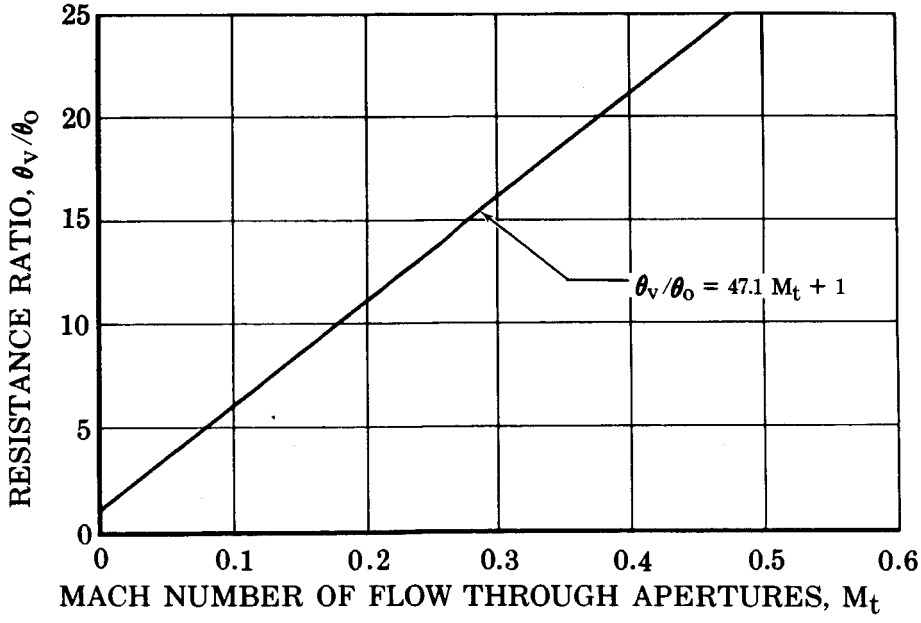

Figure IV-7. Resistance Ratio vs Mach Number, Flow-Through Apertures

FD 21983B

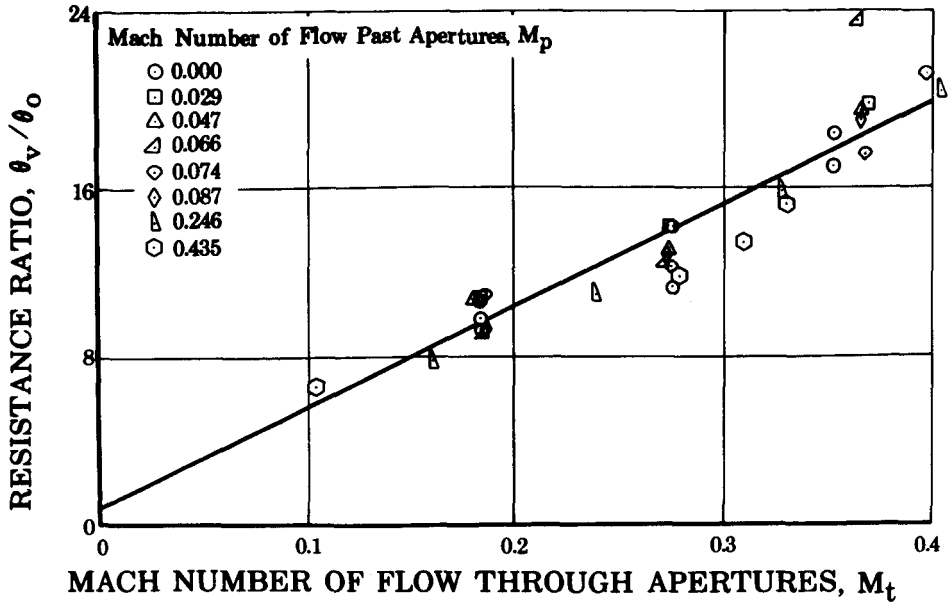

Figure IV-8. Results of Simultaneous Flow Experiment FD 21981A

It is possible that precise acoustic resistance data with low simultaneous flows can be obtained; however, a much more sophisticated flow control system than the one presently available would be necessary. The effects of simultaneous flows with low gas velocities past (Mach number less than 0.10) are only of secondary importance to designers of absorbing liners for rocket motors; therefore, it is not believed that further attempts to obtain acoustic data in this flow regime are warranted.

D. RECOMMENDATIONS

Based on the results of the flow experiments the following recommendations are made:

1. For the design of absorbing liners subjected to simultaneous flows, the increase in resistance due to flow should be computed as if only flow-through were present.
2. To predict the resistance with gas flows other than air, the equations relating the increase in resistance to Mach number should be used.

SECTION V
IMPROVEMENT OF ABSORPTION CHARACTERISTICS

A. GENERAL

Combustion instability in a rocket motor can occur over the wide range of frequencies that correspond to the pure or combined modes of the combustion chamber. The absorption characteristics of an optimum acoustic liner designed for a typical oxygen-hydrogen rocket motor are shown in figure V-1. Each of the possible modes of instability is indicated by bars at the bottom of the figure. Even with an optimized design the absorption coefficient is extremely sensitive to frequency and decreases rapidly on either side of the resonant frequency. Since instability can occur in any of the possible modes, the ideal liner should have an absorption coefficient that is independent of frequency and has a value near 100%. If the bandwidth characteristics of a typical liner with circular apertures are improved, the maximum value of the absorption coefficient is usually reduced significantly. The objective of the work reported herein was to experimentally evaluate methods of increasing the absorption of acoustic liners and extend the absorption capability over a wider range of frequencies. Two basic approaches to the problem were selected. The first was to evaluate the feasibility of integrating different resonator configurations into one design. This approach was an attempt to produce multiple resonant frequencies and, therefore, maximum damping capability for the various modes of instability. The second approach was directed toward improving absorption capability of the single resonator configuration, which was to be accomplished through redesign of the resonators and through usage of various porous materials.

B. LINER WITH DIFFERENT CAVITY VOLUMES

Absorbing liners of the Helmholtz array type are usually designed with the same cavity volume for each resonator. With such a design, resonance and therefore peak absorption can occur at only one frequency. However, a liner can be constructed with several different cavity volumes so that, theoretically, resonance occurs at more than one frequency. That is, the liner can be "tuned" so that good absorption is obtained at all the dominant frequencies of a particular combustion chamber.

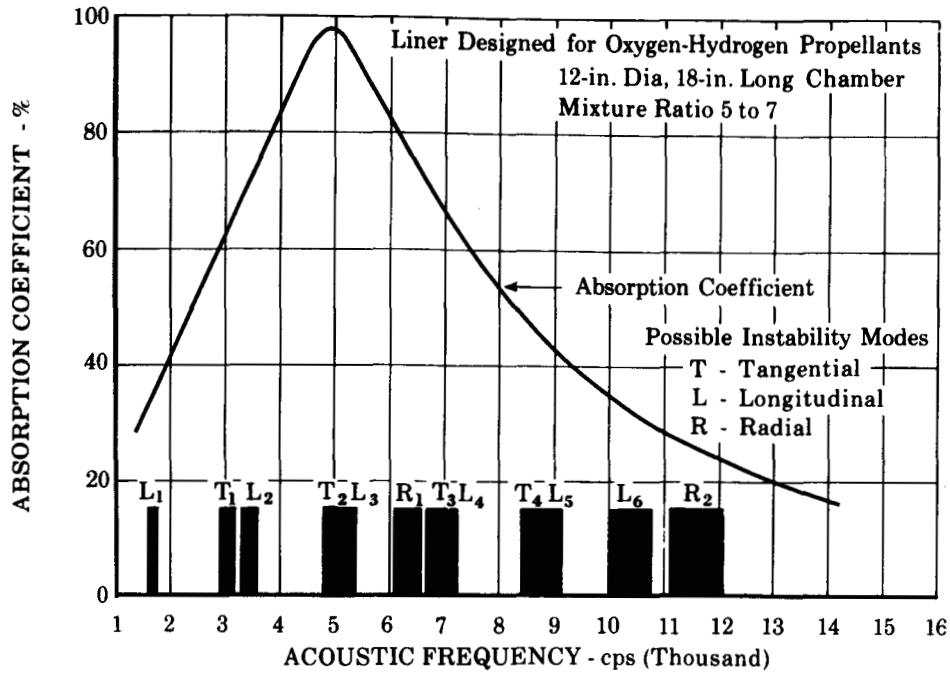

Figure V-1. Results of Liner Design Study FD 14206B

To investigate the technique experimentally, the four liner samples described in table V-1 were fabricated and tested in the impedance tube.

Table V-1. Liner Samples (Different Cavity Volumes)

Sample Number	Design Frequency - Hz	Backing Distance - in.
1	2000	0.255
2	1600	0.399
3	1200	0.710
4	2000, 1600, 1200	0.255, 0.399, 0.710

Each sample was 0.250-in. thick and had an open area ratio of 3%, with apertures of 0.07-in. diameter. Samples No. 1 through 3, which were used to supply control data, were conventional Helmholtz resonators (see figure V-2), each designed for maximum absorption at the particular frequency listed in table V-1. Sample No. 4 had three differently sized backing cavity volumes (see figure V-2) that were designed so that one-third of the resonators would be at resonance at each of the design frequencies. A typical cavity volume plate for samples No. 1 through No. 4 is shown in figure V-3. The combination cavity volume and backing plate for sample No. 4 is shown in figure V-4.

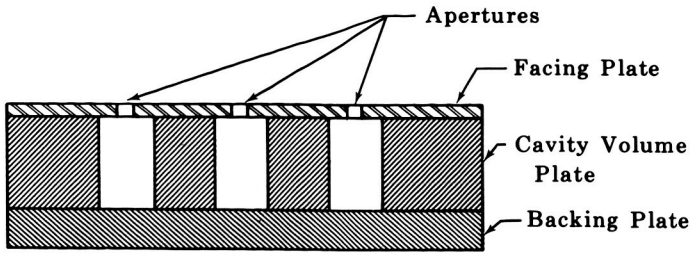

Helmholtz Resonator Control Sample

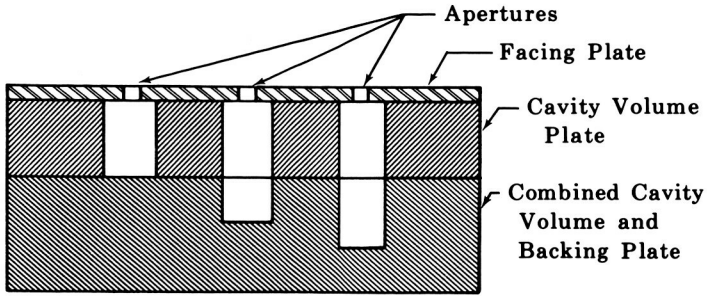

Resonant Sample With Different Cavity Volumes

Figure V-2. Helmholtz and Composite Volume Samples FD 23132

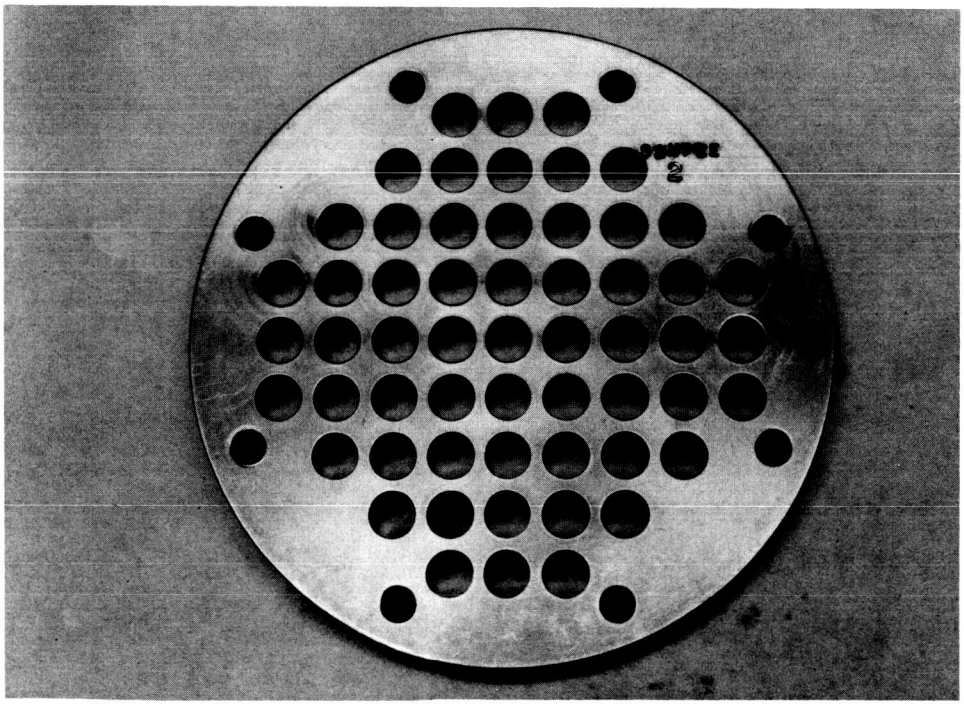

Figure V-3. Cavity Volume Plate for Sample No. 2 FE 60842

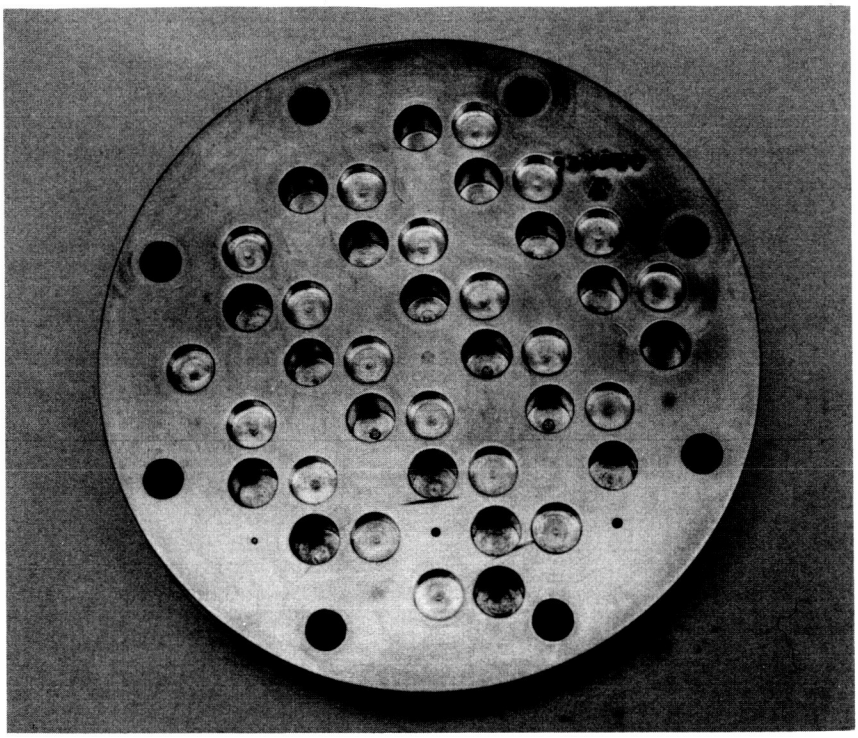

Figure V-4. Combination Cavity Volume and Backing Plate for Sample No. 4 FE 60846

A series of tests was conducted at a constant SPL of 134 db to determine the bandwidth performance of each sample. The data from samples No. 1 through 3 were compared with those from sample No. 4. The results are shown in figure V-5. Note that the bandwidth performance of the composite sample (No. 4) is significantly better than that of the control samples, i.e., the combination cavity volume sample has an absorption coefficient that is almost constant over the design resonant frequency range. At some frequencies the composite sample has higher absorption values than any of the control samples due to a superimposing effect produced by more than one type of absorber operating at that frequency. Normally, the composite sample absorption in a particular frequency range is influenced most by the resonator type most effective within that range.

The results of the tests indicate that the bandwidth of a liner can be significantly improved by tuning the resonators for the desired frequencies. Although the composite sample was tuned for only three frequencies, it may be concluded that using the same technique a liner could be designed to provide sufficient absorption values over a wide band of frequencies.

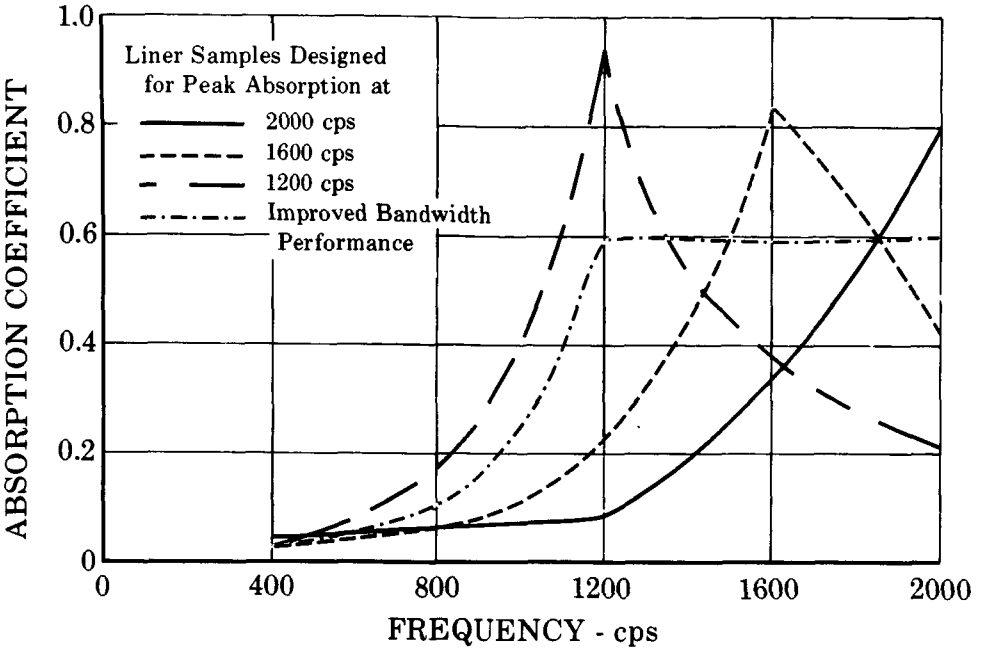

Figure V-5. Results of Bandwidth Analysis for Sample With Different Cavity Volumes FD 18286

C. HIGH-RESISTANCE APERTURES

One type of high-resistance aperture is a conventional Helmholtz resonator with a porous material inserted immediately behind the sample. The porous material increases the aperture resistance and dissipates additional energy while possibly increasing the bandwidth characteristics of the system.

To test the concept, Feltmetal samples were installed behind standard resonator array samples and the absorption coefficients of the assemblies were measured. The resonator samples alone were tested first with a 0.500-in. cavity to obtain control data. The samples were then tested with the 0.250-in.-thick Feltmetal plates installed immediately behind them and separated from the rear of the cavity by 0.250 in. In table V-2 a description of the resonant samples is given. Three Feltmetal plates with densities of 10, 20, and 30% were used with each resonator sample. A total of 20 tests was conducted; the frequency range was 400 to 2000 Hz for each test.

Table V-2. Description of Resonant Samples

Sample Number	Aperture Diameter - in.	Thickness - in.	Open Area Ratio - %
1	0.052	0.0625	1.2
2	0.052	0.125	1.2
4	0.052	0.250	5.34
5	0.070	0.250	5.34
6	0.0995	0.250	5.34

Experimental results are shown in figures V-6 through V-10 in which the absorption coefficients have been graphed versus frequency. The two samples with the lowest open area ratio, 1.2% (figures V-6 and V-7) are seen to have flat frequency response characteristics with each of the porous plates installed; however, the maximum absorption coefficients are much lower than those of the resonator alone. Apparently, the combination of low sample open area ratio for the resonant sample and high density Feltmetal backing plates acted effectively as a solid facing to the incident-plane sound wave. The impedance of the resonator assembly, therefore, consisted principally of the orifice resistance and the contributing porous plate resistance term. These largely resistive configurations approached in theory a solid wall configuration that possesses an infinite resistance and zero acoustic absorption.

The data from the samples with 5.34% open area are shown in figures V-8, V-9, and V-10. Again the two highest density porous plate assemblies (20 and 30%) significantly reduced absorption coefficient amplitude. The reduction was of such a degree that no bandwidth performance could be realized. Again the resistance has become the dominating term of the equivalent impedance, resulting in small absorption values. However, significant results were obtained from the less dense porous plate (10%) combined with the 5.34% open area resonator sample. Absorption amplitudes approached those of the control sample and an improved bandwidth performance was obtained over the frequency range.

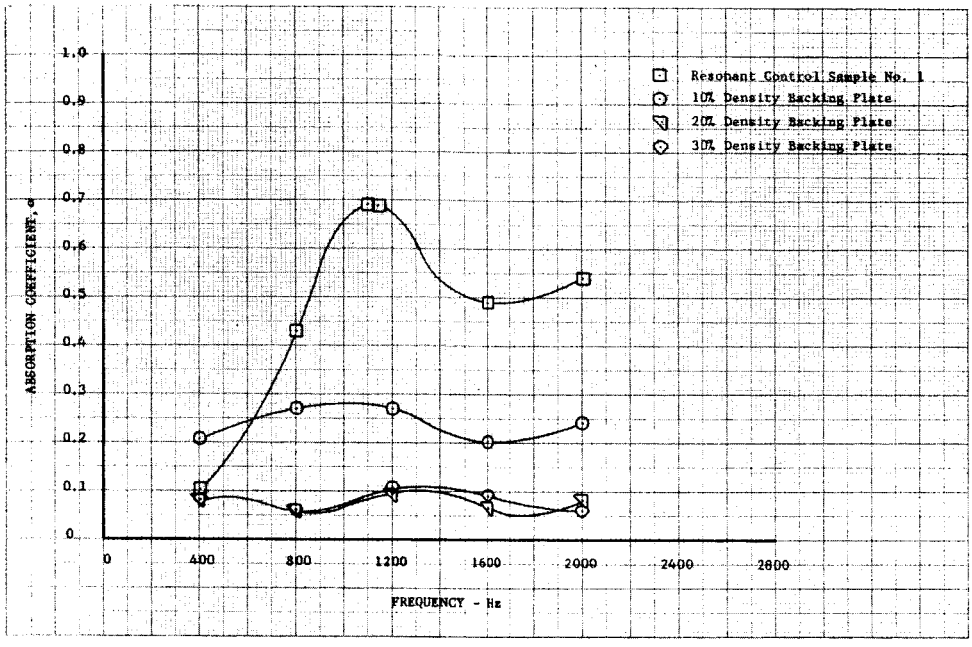

Figure V-6. Absorption vs Frequency for Resonant Sample No. 1 and High-Resistance Aperture Samples

DF 59559

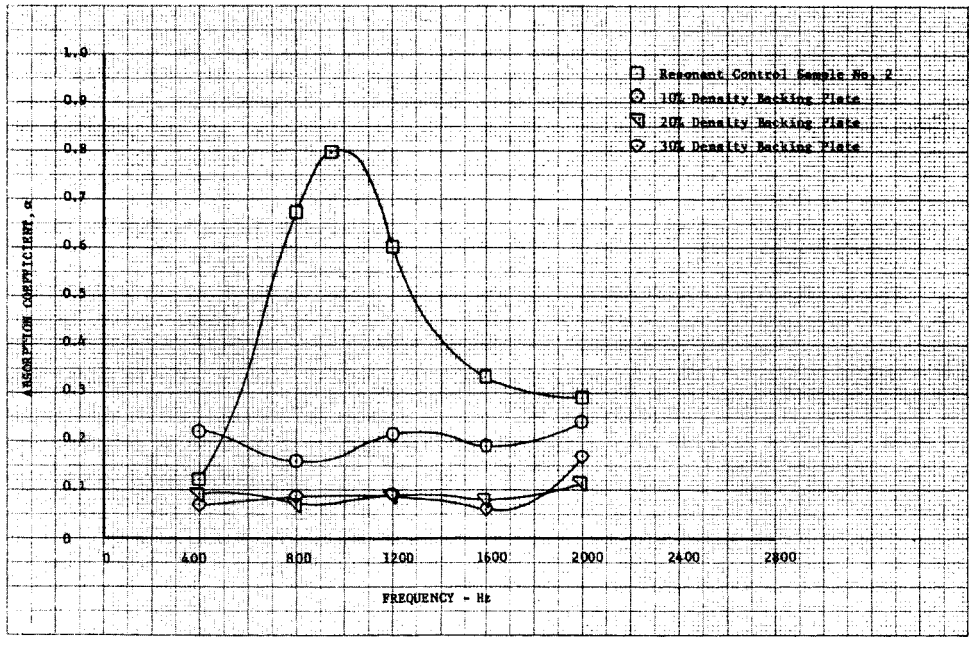

Figure V-7. Absorption vs Frequency For Resonant Sample No. 2 and High-Resistance Aperture Samples

DF 59560

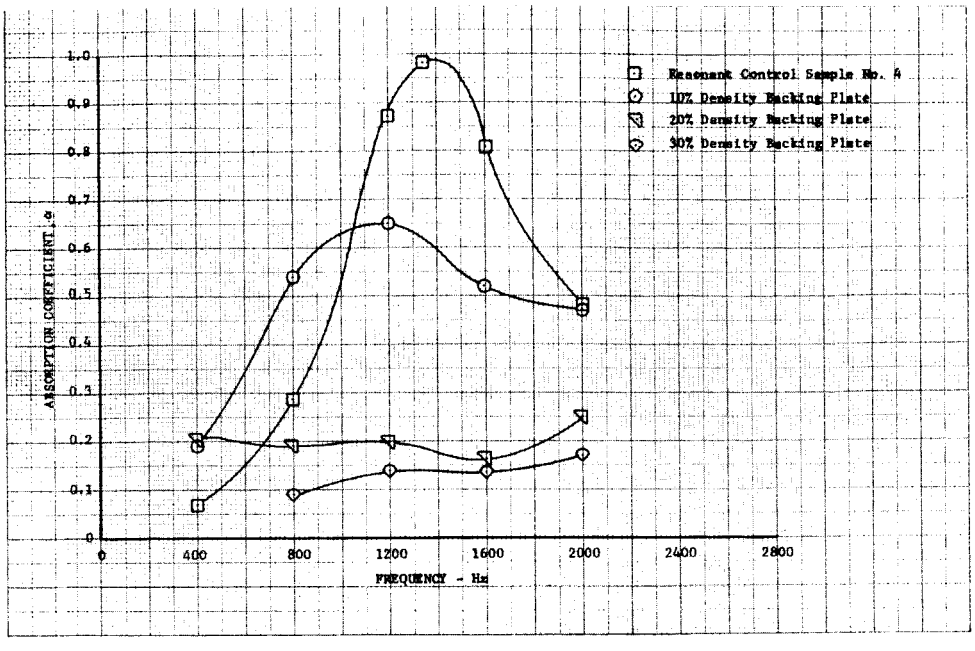

Figure V-8. Absorption vs Frequency for Resonant Sample No. 4 and High-Resistance Aperture Samples

DF 59561

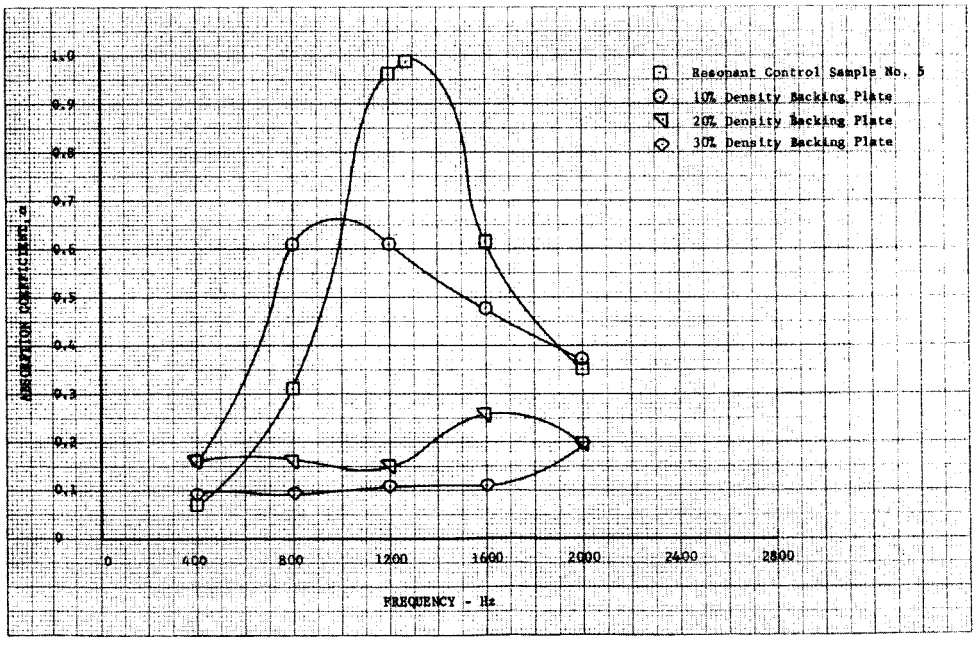

Figure V-9. Absorption vs Frequency for Resonant Sample No. 5 and High-Resistance Aperture Samples.

DF 59562

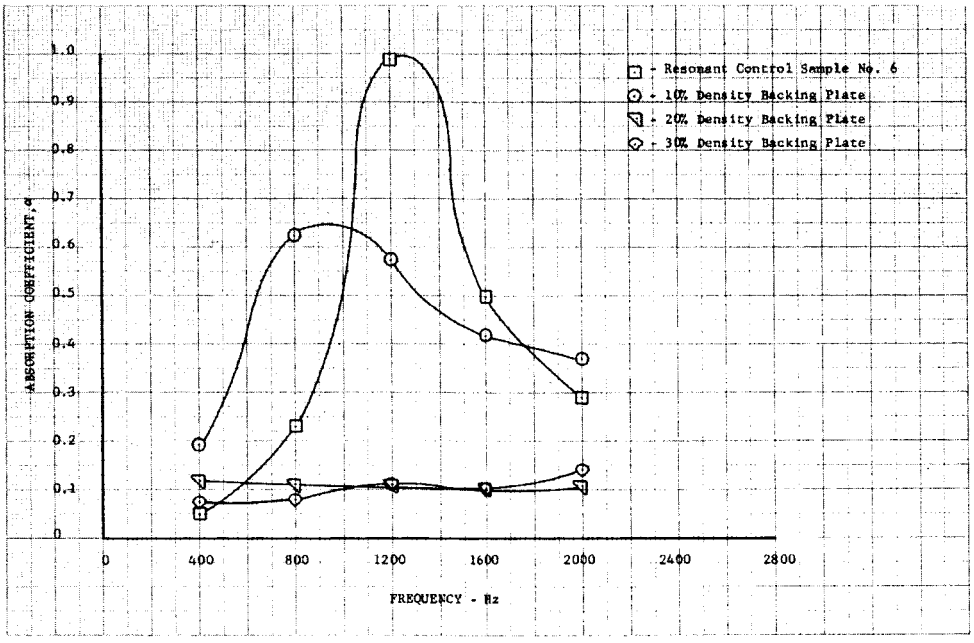

Figure V-10. Absorption vs Frequency for Resonant Sample No. 6 and High-Resistance Aperture Samples DF 59563

The results from this series of tests indicate that high resistance apertures constructed of conventional resonator arrays and porous backing plates do affect total absorption values and bandwidth performance. The combination of low resonator open area and high density backing plates offers no significant improvement over the resonant array by itself. However, a lower density backing plate combined with larger open areas does offer improved bandwidth performance with a slight sacrifice in absorption coefficient amplitude.

D. NONRESONANT ABSORBERS IN THE FORM OF CONVENTIONAL RESONATORS

A conventional resonant absorber can be described as an array of Helmholtz resonators; a nonresonant absorber is defined as a porous absorber (other than a perforated plate) that has a backing volume. The acoustic resistance of a nonresonant liner can be controlled by changes in wire size and porosity thus varying the acoustic absorption coefficient. The absorption characteristics can possibly be further improved by drilling conventional apertures in nonresonant samples. To evaluate the scheme nonresonant porous samples were constructed of Rigimesh material and tested in the impedance tube. Table V-3 gives a complete description of each sample; a typical sample is shown in figure V-11.

Table V-3. Description of Rigimesh Samples

Sample Number	Rigimesh Rating - scfm	Aperture Diameter - in.	Sample Thickness - in.	Open Area - %
1A	30	0.052	0.0625	1.2
2A	30	0.052	0.125	1.2
4A	300	0.052	0.25	5.34
5A	300	0.070	0.25	5.34
6A	150	0.0995	0.25	5.34

Control data used as a basis for comparison were obtained from standard resonant samples with identical open area ratios and aperture thicknesses. All tests were conducted with a constant backing depth of 0.500 in.

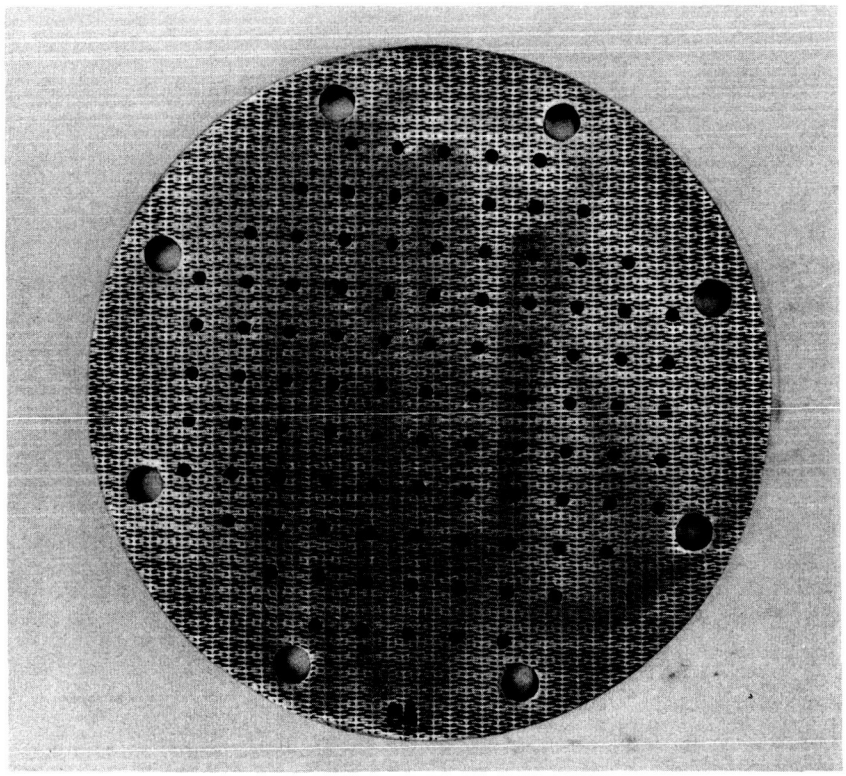

Figure V-11. Liner Sample No. 5A FE 60714

The results of the impedance tube tests are shown in figures V-12 through V-16. For each set of tests the maximum absorption amplitude remained constant between the nonresonant and control samples. Although only a slight improvement in bandwidth characteristics is noted, the

frequency at which the peak absorption occurred was shifted to a lower frequency with one of the samples (see figure V-13). The frequency shift was observed only with the 300-scfm Rigimesh samples. The shift in resonant frequency to a lower value is important for the following reason: in the design of absorbers for the suppression of low frequency instability (i.e., less than 800 Hz), it is usually difficult to match the resonant frequency of the liner assembly with that of the instability because the large cavity volumes that are required are not usually available. The use of a nonresonant absorber with apertures (so that the resonant frequency is decreased) would be a means to alleviate the problem.

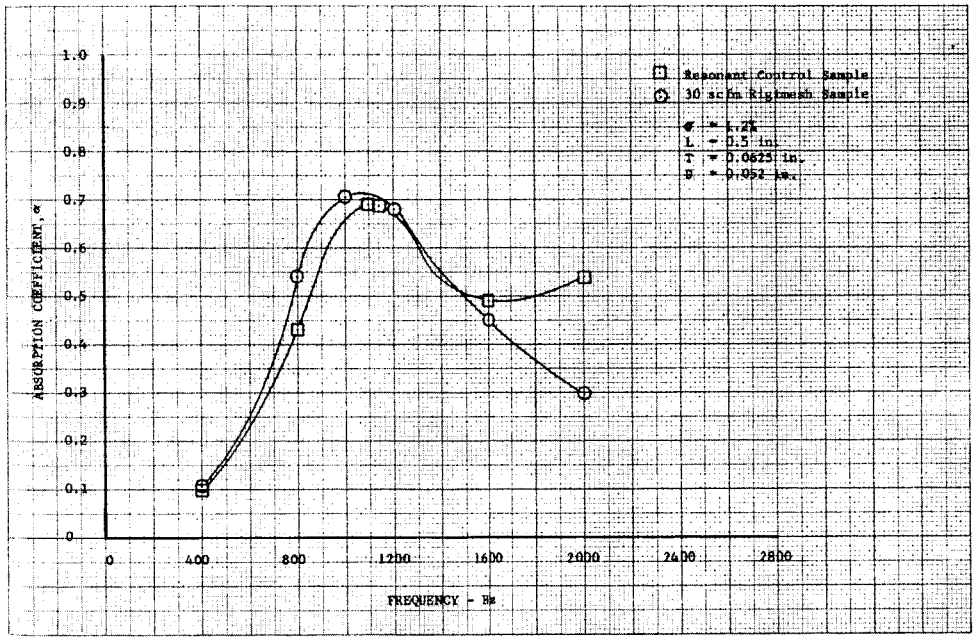

Figure V-12. Absorption vs Frequency for Resonant Sample and Rigimesh Sample No. 1A

DF 59564

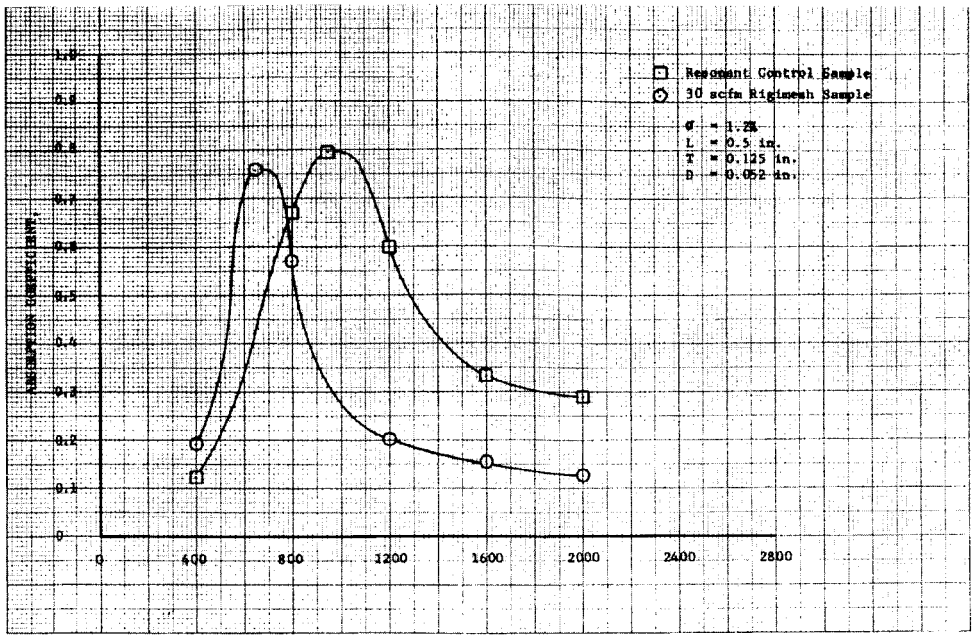

Figure V-13. Absorption vs Frequency for Resonant Sample and Rigimesh Sample No. 2A

DF 59565

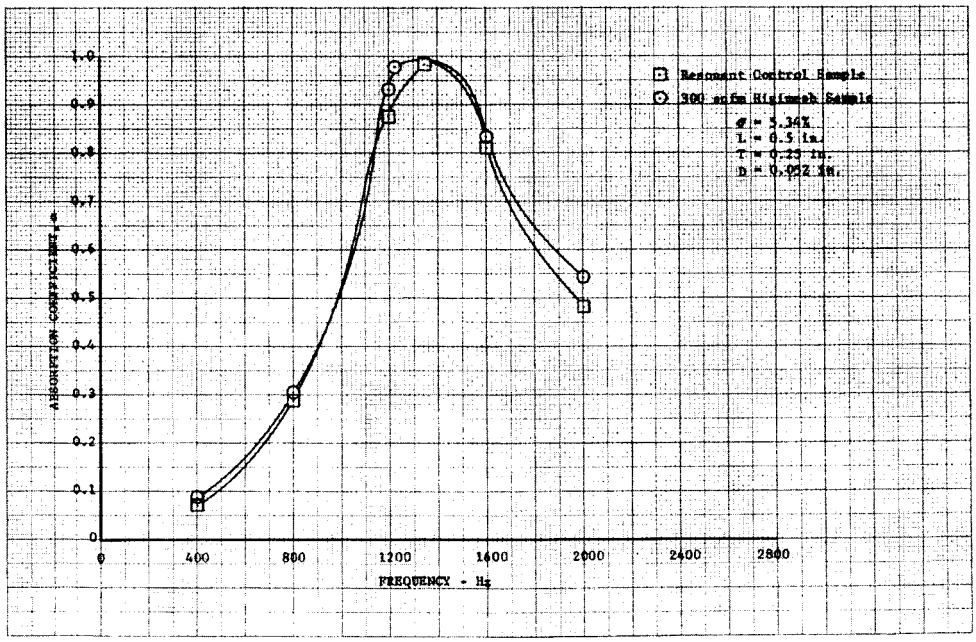

Figure V-14. Absorption vs Frequency for Resonant Sample and Rigimesh Sample No. 4A

DF 59566

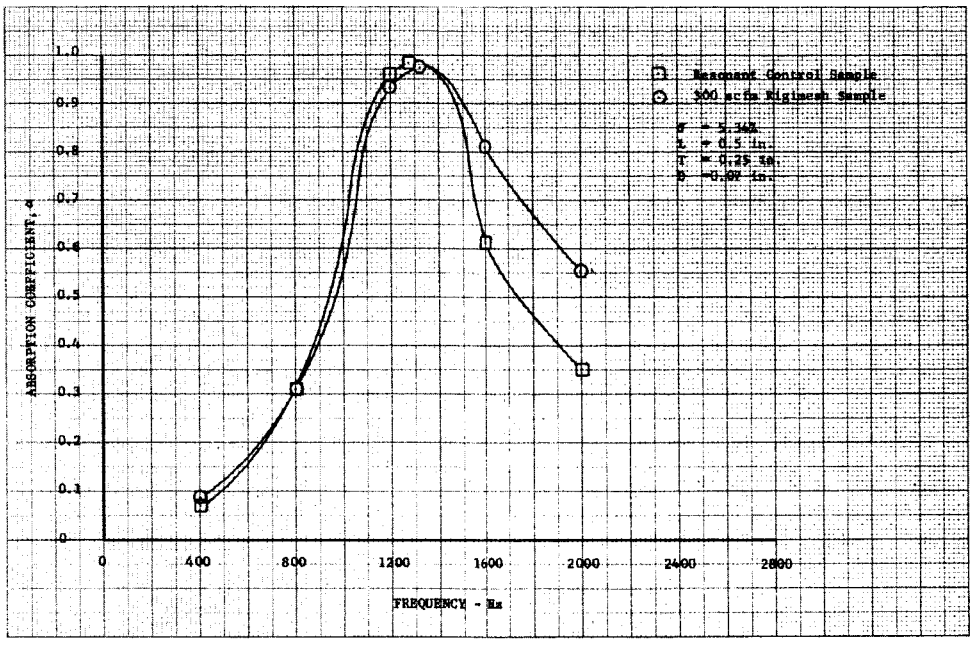

Figure V-15. Absorption vs Frequency for Resonant Sample and Rigimesh Sample No. 5A

DF 59567

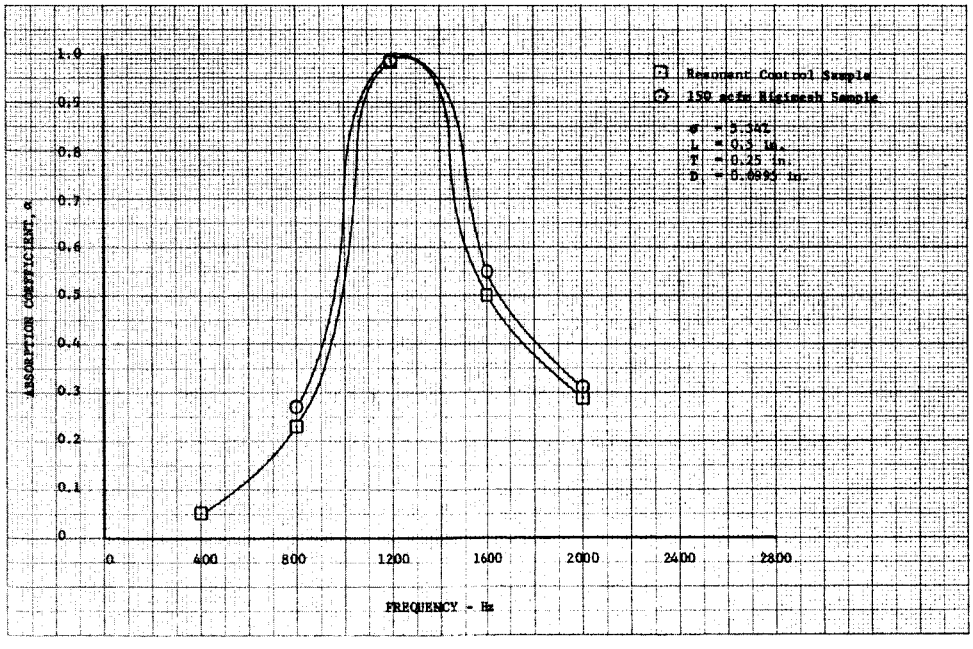

Figure V-16. Absorption vs Frequency for Resonant Sample and Rigimesh Sample No. 6A

DF 59568

E. DIMPLED RESONATORS

A dimpled sample is a conventional resonator configuration in which the apertures have been punched or lengthened to increase the effective length. Two advantages are expected to result from using the dimpled sample concept. The first is a weight advantage since a dimpled array should have the same resonant properties as a sample with a thickness equal to the aperture length of the dimple. The second possible advantage would result in the changes of the resonator's acoustic properties that occur by placing a backing plate at various distances from the dimple exit. Theoretically, a dual-orifice effect that would change the reactance of the configuration and alter its resonant properties can be created within the cavity when the gap between the plate and the aperture is small.

To evaluate the dimpled resonator concept, a 4.5% open area sample with a 0.030-in. wall thickness and 0.108-in.-long dimples was fabricated and tested (see figure V-17). Table V-4 shows the geometrical configurations considered and the various distances the plate was placed from the dimple exit.

Results of the impedance tube tests are shown in figures V-18 through V-20. The backing depth was varied, with all other resonator dimensions held constant. Data for the three configurations tested indicate good agreement of resonant frequencies between the dimpled sample and the equivalent Helmholtz resonator with an equal backing depth (figure V-21). The Helmholtz resonator, however, could also be represented by the configuration of figure V-22, using a smaller backing depth. By comparison, the dimpled resonator then has a lower resonant frequency as shown in figures V-18 through V-20, because of its increased backing volume. The slashed lines in the above figures represent the theoretical resonant frequencies for the two different backing depths; the solid curve is a plot of data obtained experimentally.

Placing the backing cavity plate at various distances from the dimpled aperture exit produced no effects on resonant properties that were different from theoretical. That is, the creation of additional apertures at the dimple exit had no effect upon the mass reactance or effective length of the resonator.

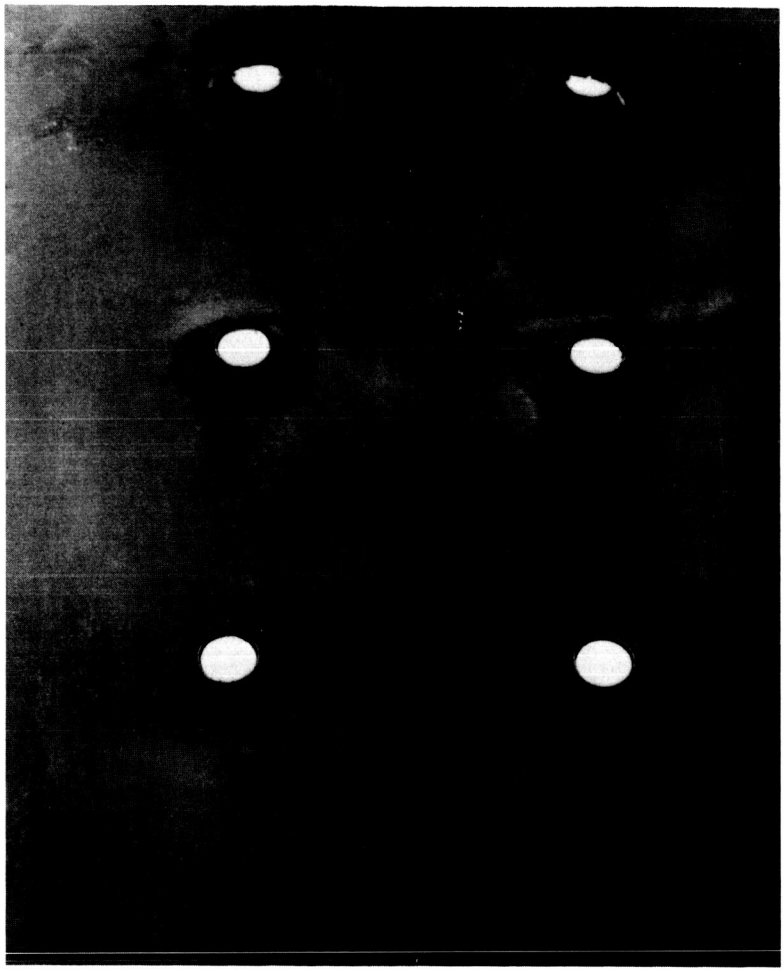

Figure V-17. Dimpled Facing Sample FC 10769

Table V-4. Geometrical Configurations Considered With a 4.5% Open Area Sample

Dimple Length - in.	Total Thickness - in.	Backing Distance - in.	Gap Between Aperture Exit and Backing Plate - in.
0.108	0.133	0.4375	0.3295
0.108	0.133	0.3750	0.2670
0.108	0.133	0.3125	0.2045

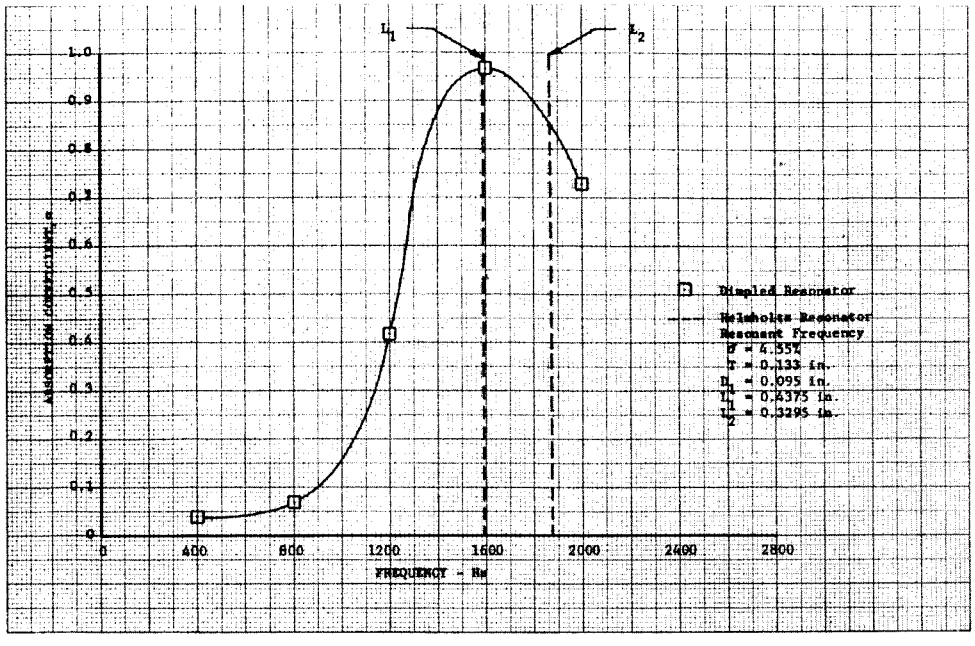

Figure V-18. Absorption vs Frequency for Dimpled Resonator Configuration No. 1 DF 59569

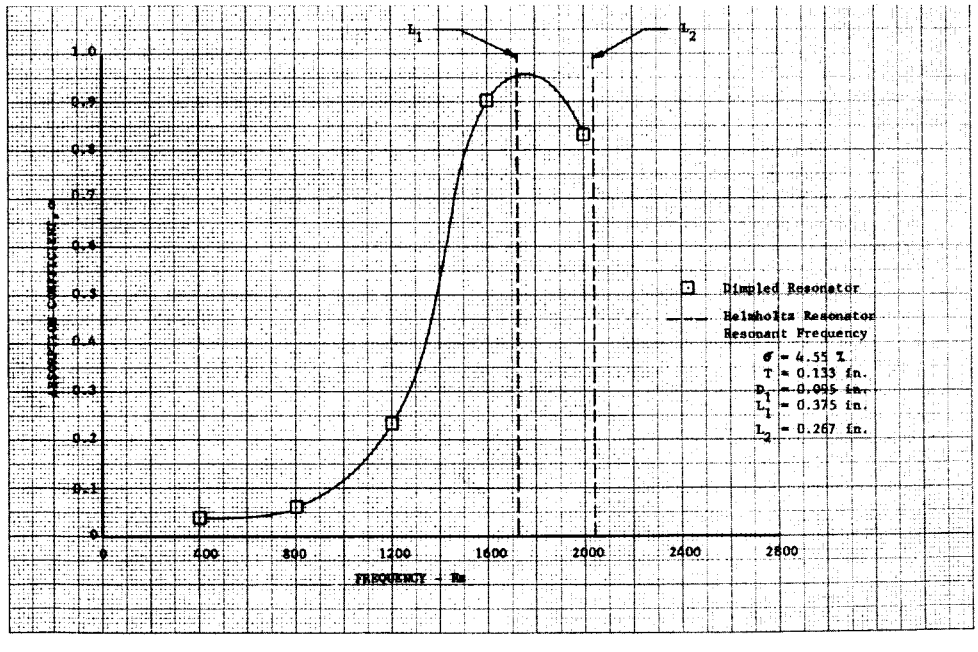

Figure V-19. Absorption vs Frequency for Dimpled Resonator Configuration No. 2 DF 59570

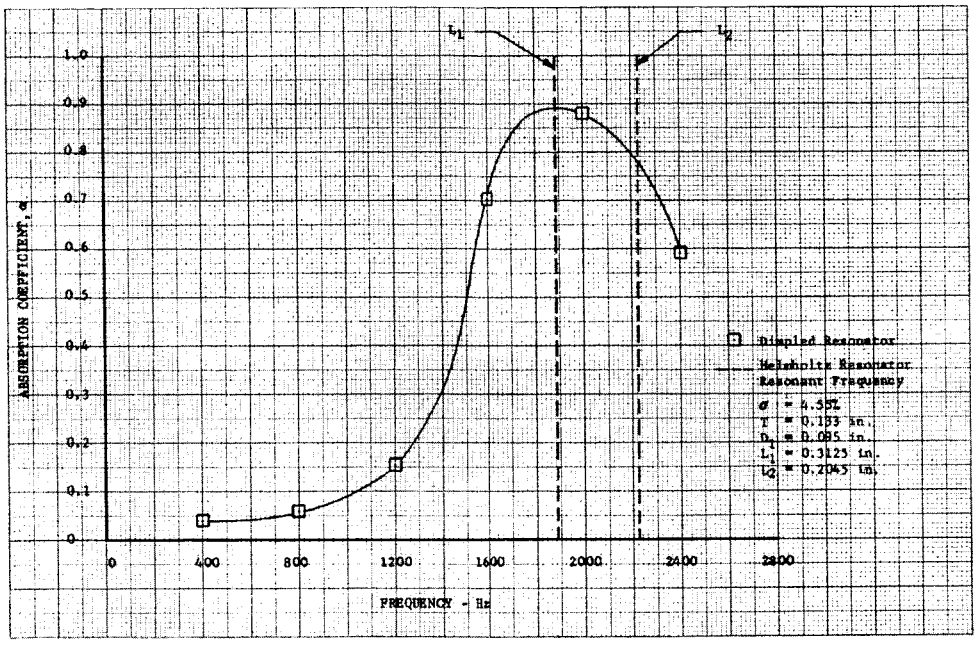

Figure V-20. Absorption vs Frequency for Dimpled Resonator Configuration No. 3 DF 59571

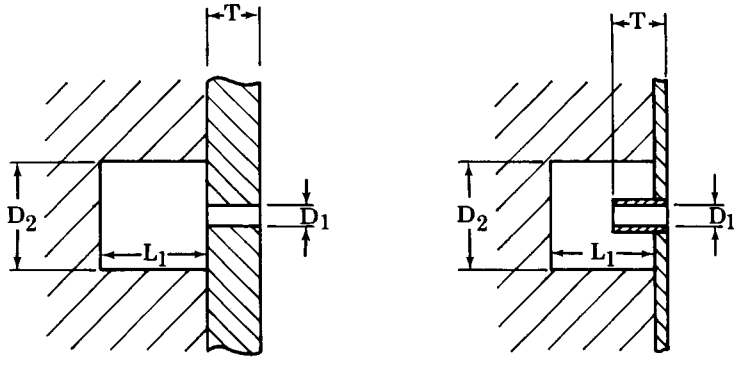

Helmholtz Resonator
Design No. 1

Dimpled Resonator

Figure V-21. Dimpled and Helmholtz Resonators, Type A FD 23052

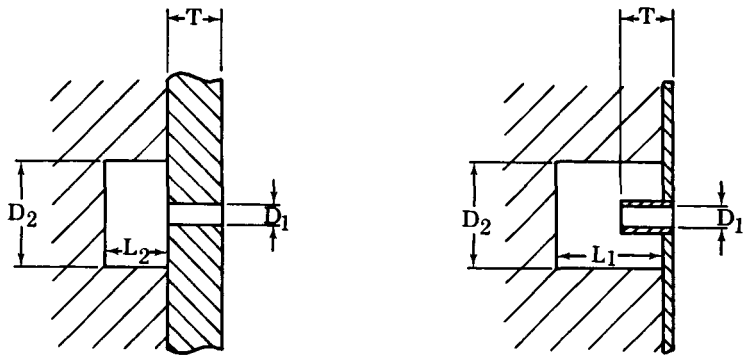

Helmholtz Resonator
Design No. 2

Dimpled Resonator

Figure V-22. Dimpled and Helmholtz Resonators, Type B FD 23053

It may be concluded that the dimpled resonator possesses absorbing characteristics that are the same as an equivalent Helmholtz resonator array. The dual-orifice effect was not observed with the samples tested. The variance of the gap between aperture exit and backing plate produced no significant changes in resonant properties or frequency bandwidth.

F. DOUBLE RESONATOR IN SERIES

A double resonator is defined as two Helmholtz resonators connected in either series or in parallel. The concept may be extended to an unlimited number of resonators that result in multiple series or parallel networks. These networks are referred to as acoustical wave filters because of their ability to block undesired frequencies. The design of networks is greatly facilitated by taking advantage of the analogy between acoustic and electrical filters. The series networks are constructed by using a combination of resistances and reactances of one type of impedance, Z_1, in series with the line and reactances of another type of impedance, Z_2, shunted across the line (see figure V-23).

The series acoustical network and the equivalent electrical circuit with Helmholtz resonator elements are given in figure V-24. Theoretically, a series of properly designed resonators could provide continuous absorption capability independent of frequency.

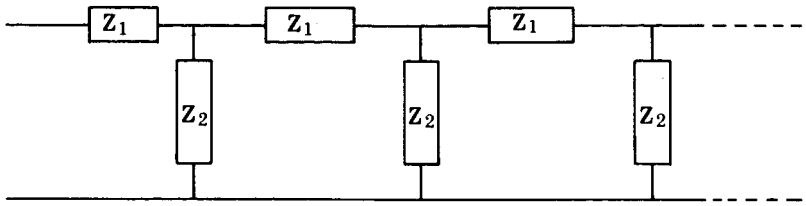

Figure V-23. Series Ladder-Type of Network Used as a Filter FD 23054

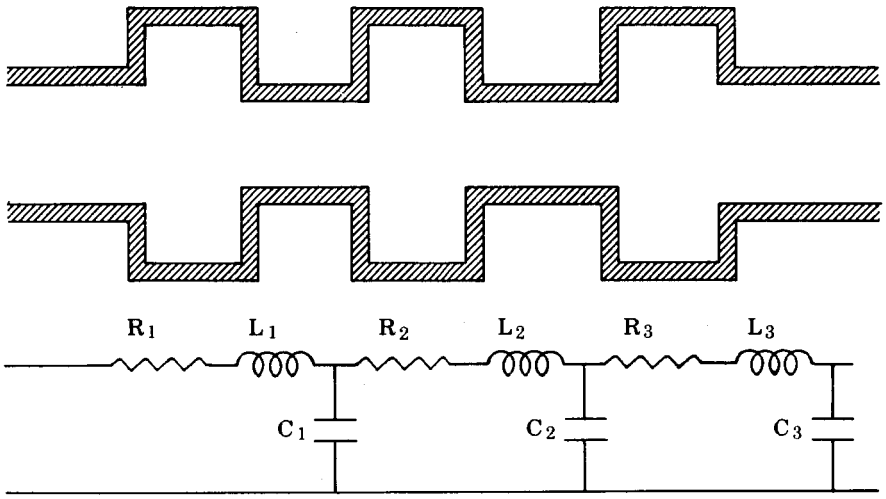

Figure V-24. Series Acoustical Circuit and Analogous Electrical Circuit FD 23055

The simplest series acoustical network would be two Helmholtz resonators (i.e., a double resonator). The bandwidth characteristics of double resonators connected in series were evaluated using the ASTM impedance tube. Each resonator was of the array type with a typical configuration arranged as shown in figure V-25. The test data of two configurations, which illustrate the most significant results, are presented. In both configurations the sample with the highest open area (10.8%) was exposed to the incident wave. The second sample with a 1.2% open area was located 0.250 in. behind the first sample and 0.250 in. from a solid wall. A complete description of the samples for both configurations is given in table V-5.

Results of the tests are shown in figures V-26 and V-27. The Configuration A series resonator was found to be a good broadband absorber. High absorption is realized from a frequency less than the natural frequency of sample No. 1 up to 2000 Hz. It is reasonable to assume that the absorption coefficient in figure V-26 will remain above 75% up to

2650 Hz. Configuration B series resonator appears to have less desirable bandwidth characteristics. The extrapolated portion of the curve is based on experimental observations of similar test data. The primary dissimilarity between the two configurations is the magnitude of the difference between resonant frequencies for each pair of samples. It was noted that as the difference in natural frequencies becomes smaller the more improved are bandwidth characteristics.

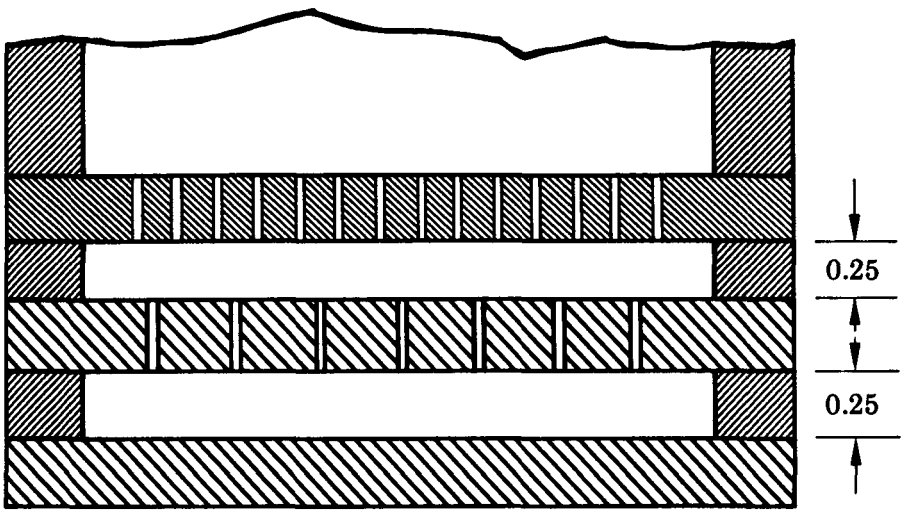

Figure V-25. Double Resonator in Series FD 22793

Table V-5. Series Double Resonator Samples

	Sample No.	Aperture Diameter - in.	Aperture Thickness - in.	Backing Depth - in.	Open Area - %	Resonant Frequency - Hz
Configuration A	7	0.052	0.250	0.250	10.8	2650
	1	0.052	0.0625	0.250	1.2	1480
Configuration B	7	0.052	0.250	0.250	10.8	2650
	8A	0.052	0.250	0.250	1.2	900

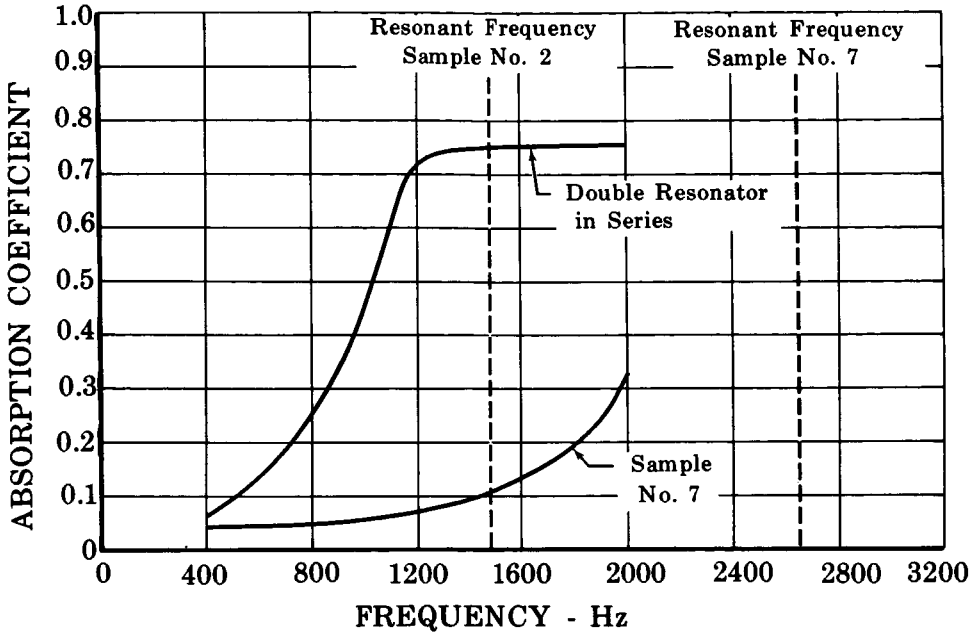

Figure V-26. Double Resonator in Series Experimental Results (Configuration-A) FD 23140

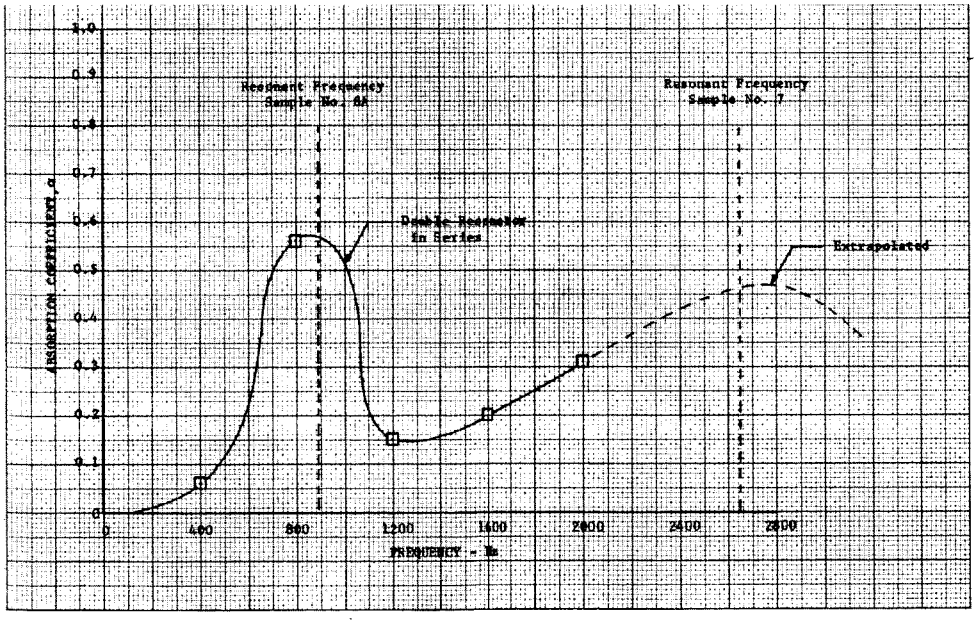

Figure V-27. Double Resonator in Series Experimental Results (Configuration-B) DF 59572

A detailed analysis of the double resonator in series is given in Appendix A. Equations that can be used to predict the equivalent impedance are presented. Experimental data indicate that the acoustical wave filter does not perform precisely as the analogous electrical wave filter, for cutoff frequencies are not as clearly defined for the acoustical elements, and continuous bandwidth absorption appears to be a function of natural frequencies of the individual resonators. However, the theory is believed to be accurate enough for absorbing liner design purposes.

G. DOUBLE RESONATOR IN PARALLEL

A second type of double resonator is the parallel combination. As with the series resonators, the system acts as an acoustical wave filter and may be represented by an analogous electrical circuit. The parallel electrical network is constructed by simply shunting the various impedances across the line as shown in figure V-28. The parallel Helmholtz resonator acoustical network and the equivalent electrical circuit with elements are given in figure V-29.

The double resonator is the simplest parallel network, combining two different types of Helmholtz configurations. The bandwidth characteristics of a double parallel sample, shown in figure V-30, were experimentally evaluated. Separate cavities were used because a common backing volume sample with different aperture diameters would not perform as a true parallel absorber.

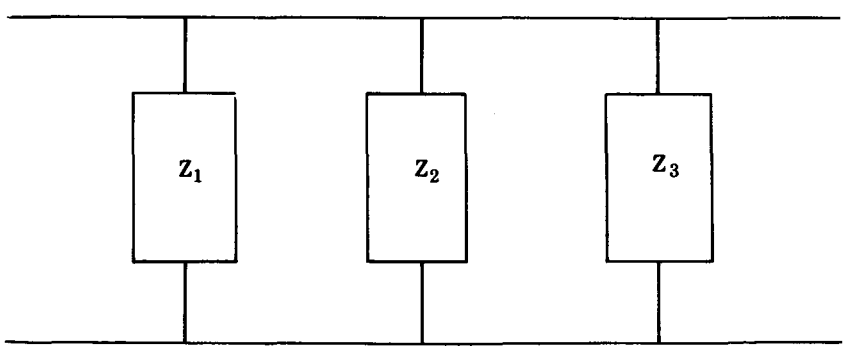

Figure V-28. Parallel Ladder-Type of Network FD 23056

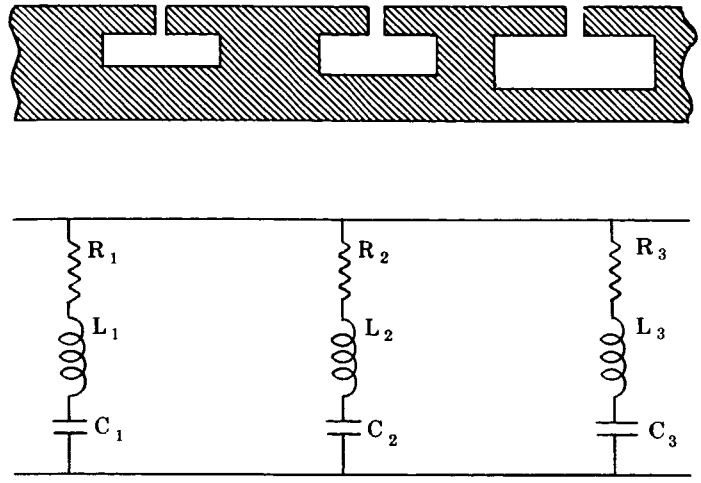

Figure V-29. Parallel Acoustical Circuit and Analogous Electrical Circuit FD 23057

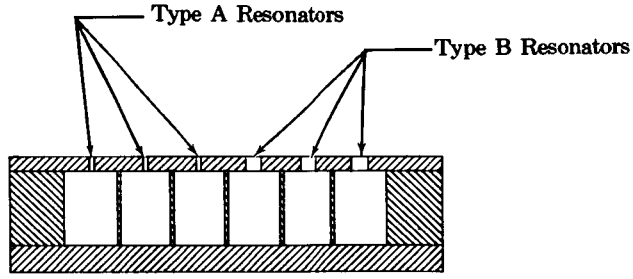

Figure V-30. Double Resonator in Parallel FD 21978

The test sample was designed with equal cavity volumes and equal backing depths for reasons of fabrication simplicity. A complete description of the geometrical configuration is given in table V-6.

Table V-6. Parallel Double Resonator Description

Resonator Type	Aperture Diameter, in.	Backing Distance, in.	Aperture Thickness, in.	Open Area Ratio, %	Resonant Frequency, Hz
A	0.070	1.100	0.250	6.4	982
B	0.140	1.100	0.250	25.0	1850

Impedance tube experiments were conducted at a constant sound pressure level over the frequency range of the test apparatus. The experimental absorption coefficients are shown in figure V-31. For comparison, the predicted results for each resonator section have also been graphed. Note that the B-type resonators have little effect on the measured absorption at frequencies lower than 982 Hz (the resonant frequency of the A-type resonators). Theory predicts that the B-type resonators have low absorption coefficients below 982 Hz; therefore, as shown in the data, the array performs as if only the A-type resonators were present in a hard wall. For frequencies above 982 Hz, the performance of the sample is influenced by both resonator types. Excellent agreement was obtained between the predicted (see Appendix B) and observed resonant frequency of the combined A-type and B-type, labeled as f_{02} in figure V-31.

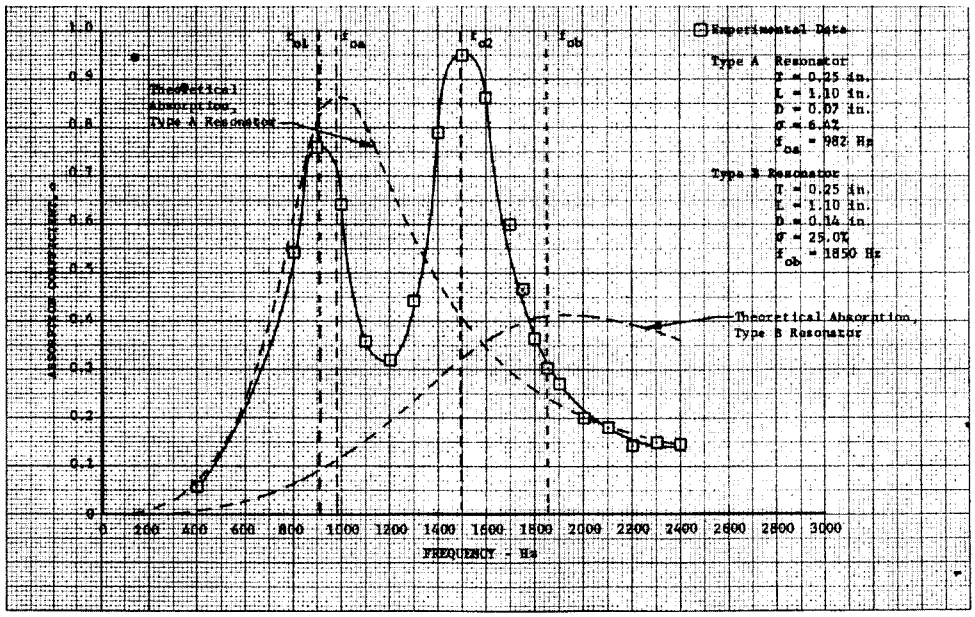

Figure V-31. Double Resonator in Parallel, Experimental Results DF 59573

An analysis of the double resonator in parallel is given in Appendix B, where equations are presented for the total equivalent impedance. Theoretically, resonant frequency equations for the parallel double resonator could be determined by setting the reactance term of total impedance equal to zero; however, the results become too cumbersome to establish resonant frequency equations in general terms. Through observation of experimental test data, however, a method of predicting resonant

frequencies was determined. The double parallel resonator appears to have double resonant frequencies. The first of these, the lower resonant frequency (f_{01}), is approximately equal to the value for the A-type resonator (f_{0A}). The second frequency at which resonance occurs lies between the values for the A-type and B-type configurations (i.e., $f_{0A} < f_{02} < f_{0B}$). For the double resonator tested, the value of f_{02} is almost a direct average of the component resonant frequencies, f_{0A} and f_{0B}. A method for computing f_{02} is given in Appendix B.

It may be concluded that a double parallel resonator of the type tested is an effective broadband absorber. An acoustic liner of this configuration would be an excellent absorber for use in rocket motor combustion chambers in which two modes of instability were inherent. Since as with the series resonator, the parallel resonator concept can be expanded to include multiple resonators, an acoustic parallel network could theoretically be designed to provide sufficient absorption characteristics for any desired frequency range.

H. CONCLUSIONS

An improvement in acoustic absorption characteristics has been sought through testing of various liner configurations in the ASTM cold-flow impedance tube. Primary objectives included extension of absorption capability over a wider range of frequencies while maintaining a sufficient absorption amplitude.

One approach to the absorption improvement objective was directed toward improving absorption capability of the single-type resonator design. The impedance tube samples tested included the following designs: high resistance apertures, nonresonant absorbers in the form of conventional resonators, and dimpled resonators. The high-resistance aperture designs constructed of conventional resonator arrays and porous backing plates (Feltmetal plates) do affect bandwidth performance and maximum absorption amplitude. The combination of large resonator open area and low density backing plate increased the frequency range over which the absorber was tested with some reduction in absorption amplitude. The nonresonant absorber constructed of a porous material with added conventional resonators produced no significant improvement in absorption characteristics; however, a resonant frequency shift was evident from the

data of one sample. This could be a desirable feature when peak absorption is required in a lower frequency mode and a conventional design is not capable of producing sufficient absorption. The dimpled resonator did not improve bandwidth performance over the conventional resonator. Primarily, the dimpled resonator offers design advantages in the areas of weight and space with no loss in absorption characteristics.

The other approach toward improving absorption characteristics was through the use of integrated resonator configurations in a single assembly. The impedance tube samples that were tested included a different cavity volume design, double resonators in series, and a double resonator in parallel. The sample with different cavity volumes produced the most significant improvement in bandwidth performance, with a slight reduction in absorption amplitude. The double resonator in parallel was found to have double resonant frequencies, an advantage that could be realized when peak absorption at two modes is necessary. The double resonator concept can be expanded to include multiple resonators, e.g., a triple resonator such as the different cavity volume sample, with multiple resonant frequencies covering the desired modes of instability. The bandwidth performance appears to be a function of the magnitude of the difference between the resonant frequencies of the individual resonators in the configuration. When the magnitude is small, as with the different cavity volume design, resonator interaction provides continuous peak absorption over the design frequency range. At present, sufficient knowledge does not exist for predicting multiple parallel resonator absorption characteristics. The analytical equations derived from electrical analogies, which are presented for the parallel resonator, are not expected to produce theoretical results exactly equivalent to experimental data; however, they are believed to be accurate enough for acoustic liner design purposes. The series double resonator performed similar to the parallel configuration, producing double resonant peaks. This design could also be extended to produce multiple resonant frequencies and therefore peak absorption at multiple modes of instability. It can be concluded that both the series and the parallel resonator designs offer advantages as an effective means to suppress combustion instability that occurs in more than one mode.

SECTION VI
PROPERTY VARIATION EFFECTS

A. INTRODUCTION

Recent rocket tests, sponsored under Contract NAS8-11038 (Reference 6), were made to develop further the theory of using absorbing liners to suppress combustion instabilities in rocket chambers. Measurements were made during these tests to determine the gas temperature in the absorbing liner aperture and cavity. Results of the tests showed that a large temperature gradient existed between the gas in the combustion chamber and the gas in the liner apertures. Such drastic temperature gradients cause substantial differences in the gas densities and sonic velocities of the chamber and liner gases. In addition, the composition of the gases could also be different if the liner is film-cooled with fuel from the outer rows of injector spuds or if the liner itself is transpiration cooled.

The objective of the property variation experiments is to determine the effects on a sound wave as it transmits across a boundary separating two gaseous mediums having completely different densities and sonic velocities. In addition, an experiment was conducted to show the effects on the performance of a liner when a change occurs in the density and in sonic velocity of the gas in the apertures and cavity.

B. TESTS WITH ASTM IMPEDANCE TUBE

A series of cold-flow tests was conducted with the ASTM impedance tube to determine how a change in gas density and sonic velocity would affect the absorption of the liner. The purpose of the experiment was to compare results of a series of tests made with nitrogen to a similar series of tests made with helium in the cavity and apertures of the absorbing liner.

All tests were made with a sample that had a nominal 5% open area ratio, a thickness of 0.250 in., and an aperture diameter of 0.050 in. A frequency range of 400 to 2000 Hz was covered and a total sound pressure level of 165 db was maintained at the sample face.

During these tests, the incident sound wave was generated in an atmosphere of gaseous nitrogen, while gaseous helium entered the cavity and apertures of the resonator (see figure VI-1). Analysis of the data revealed that the helium entering the impedance tube through the sample apertures had mixed with the nitrogen and altered the wave length of the incident sound wave, which caused a distortion in the standing wave pattern. This distortion of the wave pattern made it difficult to locate the position of pressure minimums; therefore, accurate determination of the acoustic impedance was impossible. To overcome the difficulty, an alternate method of determining the impedance of an absorbing liner was used. The method, which was suggested by the program consultant, Dr. Ingard, is described in the next paragraph.

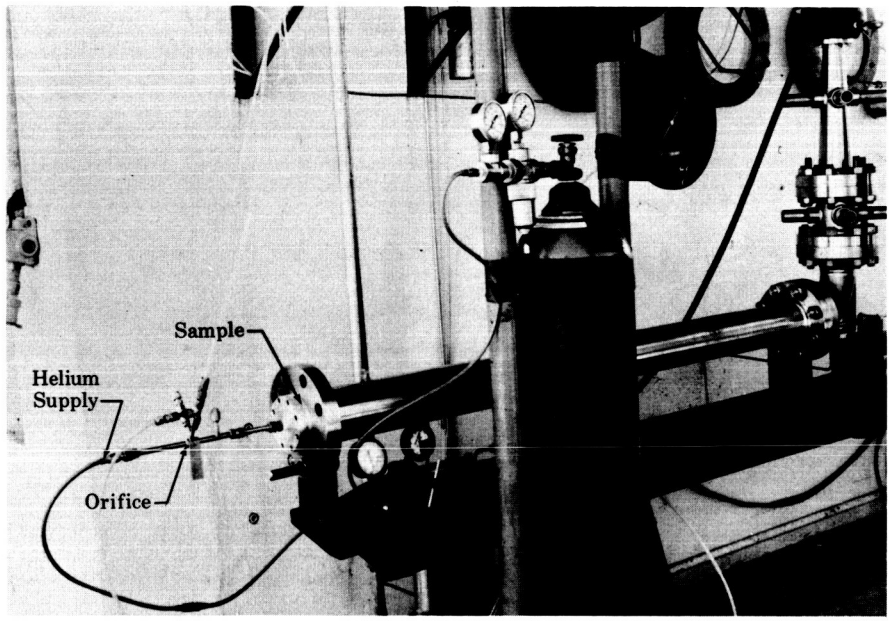

Figure VI-1. ASTM Property Variation Facility FD 20130

C. NEW PHASE ANGLE IMPEDANCE TUBE

The new impedance measuring apparatus eliminates the use of data that are based on the standing wave pattern as is needed with the ASTM tube. The new technique requires measurements of the sound pressure level at the sample face and in the backing cavity, and also the phase angle between these two pressure amplitudes.

By measuring these two pressure amplitudes, and the phase angle between them, the impedance can be determined, as shown in Appendix C, from the following equation:

$$Z = \left|\frac{P_1}{P_2}\right| \frac{1}{kL} \sin\phi - i\left[-\frac{1}{kL}\left|\frac{P_1}{P_2}\right| \cos\phi\right] \qquad \text{(VI-1)}$$

where k, the wave number is:

$$k = \omega/c = \frac{2\pi f}{c} \qquad \text{(VI-2)}$$

Also the incident sound pressure level at the sample face can be computed, as shown in Appendix D, from:

$$P_{incident} = \frac{P_1\left[(\theta+1)^2 + X^2\right]^{1/2}}{2\left[\theta^2 + X^2\right]^{1/2}} \qquad \text{(VI-3)}$$

where ϕ, the acoustic resistance is:

$$\phi = \frac{1}{kL}\left|\frac{P_1}{P_2}\right| \sin\phi \qquad \text{(VI-4)}$$

and X, the acoustic reactance is:

$$X = -\frac{1}{kL}\left|\frac{P_1}{P_2}\right| \cos\phi \qquad \text{(VI-5)}$$

The phase angle impedance tube (figure VI-2) was designed to operate over a frequency range of 0 to 10,000 Hz; the upper limit was determined by the standards set forth by the American Society for Testing Materials (Reference 5). However, because of the limited range of the driver (loudspeaker), the actual frequency range is only 500 to 8000 Hz. An Altec 290E driver is used as the sound source; an incident output of over 150 db is obtained. Two Bruel and Kjaer 1/4-in. condenser microphones (Type 4136) are used to measure the sound pressure amplitudes at the sample face and in the backing cavity. Figure VI-3 shows the instrumentation used with the above equipment. A General Radio wave analyzer is used to convert the signal from the microphones to decibels. An AD-YU phase meter (Model 524A3) is used to measure the phase angle between the two microphone outputs; a Hewlett Packard dual beam oscilloscope (Type 132A) can be used as an alternative, but less accurate, means of measuring the phase angle.

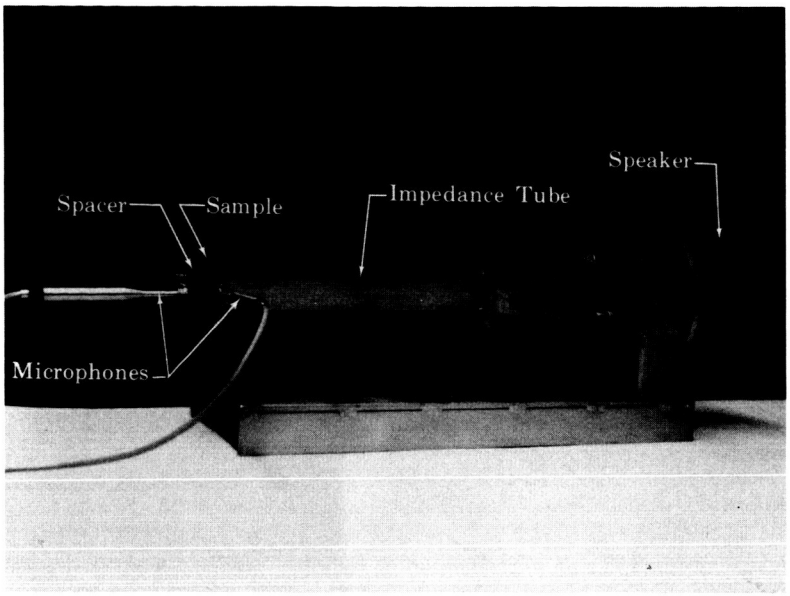

Figure VI-2. High Frequency Phase Angle Impedance Tube FD 23058

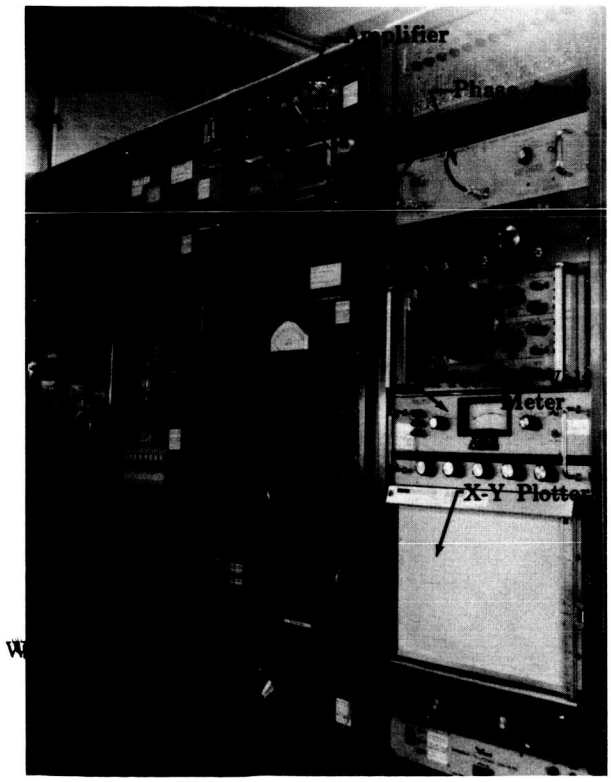

Figure VI-3. Test Stand Instrumentation FD 23059

D. TEST PROCEDURES

The first test conducted was to determine the effects on a pressure wave as it crossed a boundary between air and helium gases. To perform these tests the impedance tube was separated as shown in figure VI-4. Helium was then forced slowly into the resonator cavity, which allowed the helium to flow through the impedance tube and out the gap between the flanges, thereby leaving the air in the tapered section undisturbed. Thus, a boundary between helium and air existed across the gap formed by the separated flanges.

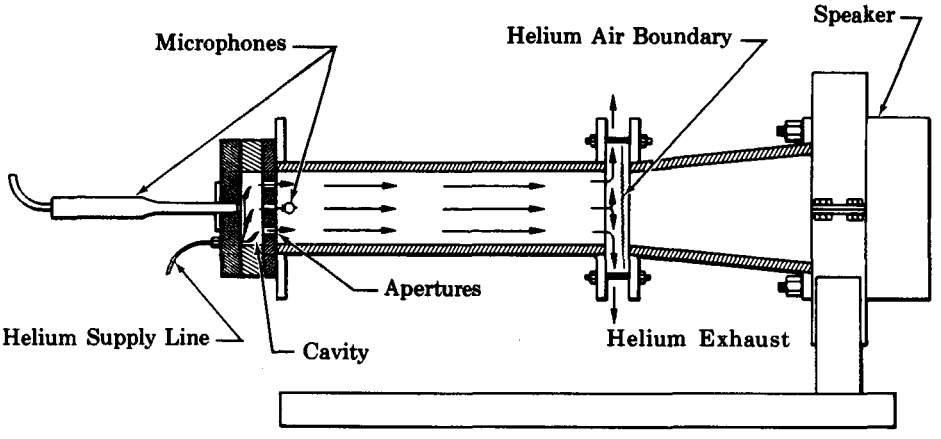

Figure VI-4. Rig Schematic for Property Effects Experiment FD 23060

During the tests the following procedure was used. The apparatus was first purged with air so that no helium was present. A voltage was then applied to the loudspeaker, causing a sound wave to be transmitted into the tube. The impedance was measured using the technique described in paragraph C. Without altering the voltage supplied to the speaker, thereby maintaining the same incident sound wave, the helium was slowly purged into the cavity, forming the helium-to-air boundary shown in figure VI-4. The same sound energy that was previously incident upon the sample when only air was in the tube was now striking the boundary between the helium and air. The sound energy after passing through the boundary became the incident wave on the sample and was measured using the same technique as before. The amplitude of this incident sound

wave was then compared to the known amplitude of the wave that was incident on the air-to-helium boundary. The difference was a measure of the attenuation caused by traversing a boundary between two gaseous mediums having different densities and sonic velocities.

All tests were made with a sample having a nominal open area ratio of 10%, a thickness of 0.10 in., and aperture diameter of 0.050 in. Tests were conducted over a frequency range of 500 to 5500 Hz, with an incident sound pressure of 145 db generated at the exit of the tapered section.

An additional test was made to determine the effects on the performance of a liner if the density and sonic velocity of the gases in the apertures and cavity were to differ from the assumed values used to design the liner. The tests were made with a closed system (figure VI-2), i.e., one in which there was no gap between the flanges. The entire inside of the impedance tube was purged with helium so that a pure helium atmosphere existed from the speaker to the resonator cavity. The impedance of the sample was then determined over a frequency range from 700 to 7000 Hz at a total sound pressure level of 151 db as measured at the sample face.

E. RESULTS

The first test was conducted to determine the effects on a sound wave as it traversed across a boundary separating helium and air atmospheres. Experimental results showed that an average drop in the sound pressure level of 3.6 db occurred when the wave passed from air into a helium atmosphere. A theoretical method based on a one-dimensional analysis, equation (VI-6), predicted a maximum drop of 4.8 db across a well-defined, air-to-helium boundary (Reference 8).

$$SPL = 20 \log \frac{2\ (\rho c)_{He}}{(\rho c)_{air} + (\rho c)_{He}} \qquad \text{(VI-6)}$$

The deviation can be attributed to the fact that, as intended, a well-defined boundary was not achieved, but a gradual change occurred between the gases within a zone that was a mixture of both air and helium.

The additional test determined the effects on the absorption of a liner when the gas properties varied; results of the test are shown in figure VI-5. The figure compares both the experimental and theoretical predicted results for the liner when it is operating in an atmosphere of either air or helium.

As seen, the resonant frequency of the liner was altered considerably when the air atmosphere was changed to helium. But the theoretical curves indicate that the performance of the liner can be predicted, at least up to the resonant frequency, as long as the gas properties in the apertures and cavity of the resonator are known.

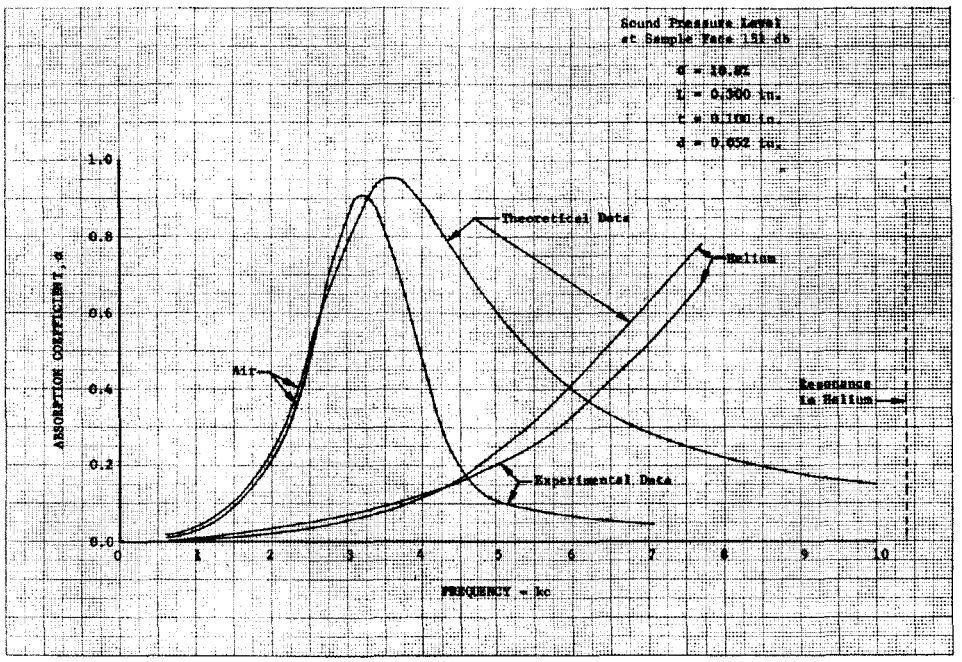

Figure VI-5. Results of the Variation in Gas Properties DF 59701

Results of these and other tests made with an air atmosphere show that when the present prediction method is used a disagreement will occur between theoretical and experimental results at frequencies greater than resonance. The disagreement is due to inaccuracies in the nonlinear correction term that must be extrapolated from data obtained at frequencies below 2000 Hz and used in the theoretical prediction method. Results of a test made with a resonator with a lower resonant frequency than the one used in figure VI-5 are shown in figure VI-6 to show how the experimental nonlinear correction term differs from the theory. In the following section, figure VII-6 shows how the use of the present method of predicting the nonlinear correction term will cause the theoretical resistance to significantly differ from the experimental value at frequencies above resonance.

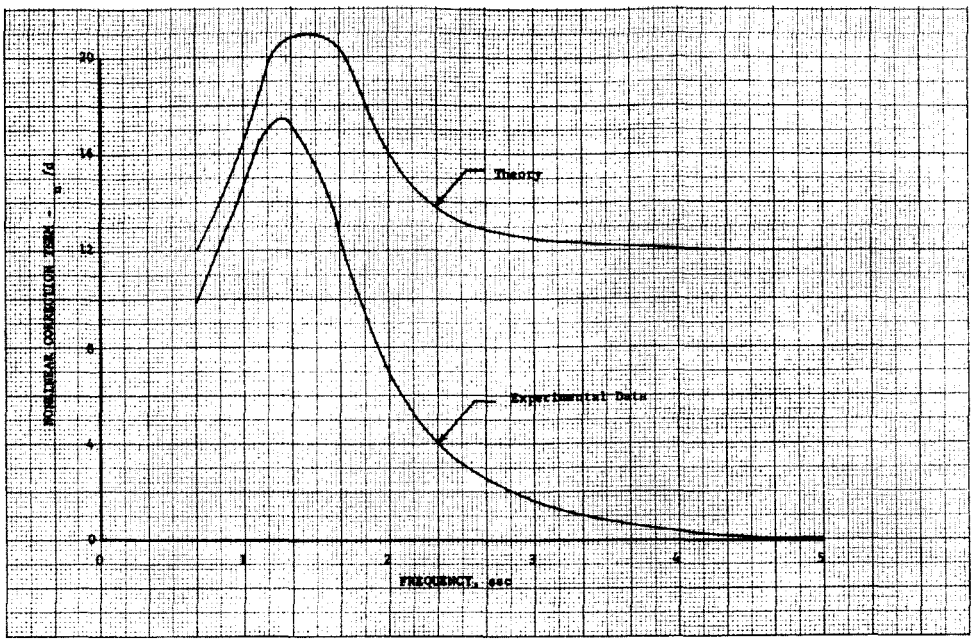

Figure VI-6. Comparison of the Nonlinear Correction Term Between the Present Theory and Experimental Data

DF 59906

F. CONCLUSIONS

From the results of the property variation experiments, it is concluded that the effects on sound intensity of a change in the medium through which a sound wave must travel can be predicted from one-dimensional theory. In addition, if the properties of the gas in the apertures and cavity of an absorbing liner operating in such an environment are known, the acoustic performance of the array can be predicted within the limits of the present theory.

SECTION VII
HIGH FREQUENCY INVESTIGATIONS

A. INTRODUCTION

In this section a description is given of additional work that was accomplished with the high frequency impedance tube. In addition, a detailed description of the phase angle impedance technique is presented. Experimental results are compared with the present theoretical prediction methods to show that disagreement occurs at high frequencies.

B. PHASE ANGLE IMPEDANCE TUBE TECHNIQUES

The phase angle impedance tube is used for determining the acoustic impedance and absorption coefficient of liner samples. The equipment consists of a short tube of fixed length and uniform cross section, with rigid walls that transmit negligible sound energy. Unlike the ASTM impedance apparatus, the tube can be made as short as desired without imposing a frequency limit. At one end of the tube, a source of sinusoidal plane waves is placed, and at the other end the specimen to be tested is placed (see figure VI-2). The tapered section between the tube and the sound source is used as a reducer so that the cross-sectional area of the speaker mouth would conform with that of the tube. An audio oscillator (signal generator) drives the loudspeaker, which transmits plane waves longitudinally along the tube.

When the longitudinal wave is incident on the sample at the end of the tube, part of its energy is reflected back up the tube in the form of another pressure wave. The incident and reflected waves set up a standing wave in the tube that has a maximum pressure amplitude at the sample face. A small microphone mounted flush in the side wall of the tube at the sample is used to measure the maximum pressure.

The portion of the incident sound energy that is not reflected back up the tube is transmitted through the apertures and into the resonator cavity. The energy in the cavity, also in the form of sound pressure, is measured with a second microphone located on the back wall of the cavity (see figure VII-1). The outputs of both microphones are fed through a wave analyzer to a millivolt meter to indicate the relative pressure amplitudes of the sound level in front of the sample and in the

cavity. In addition, the outputs of both microphones are connected to a phase meter to determine the phase difference between the incident and transmitted waves. Using the equations derived in Appendix C, the absorption coefficient and the components of impedance can be computed from the data.

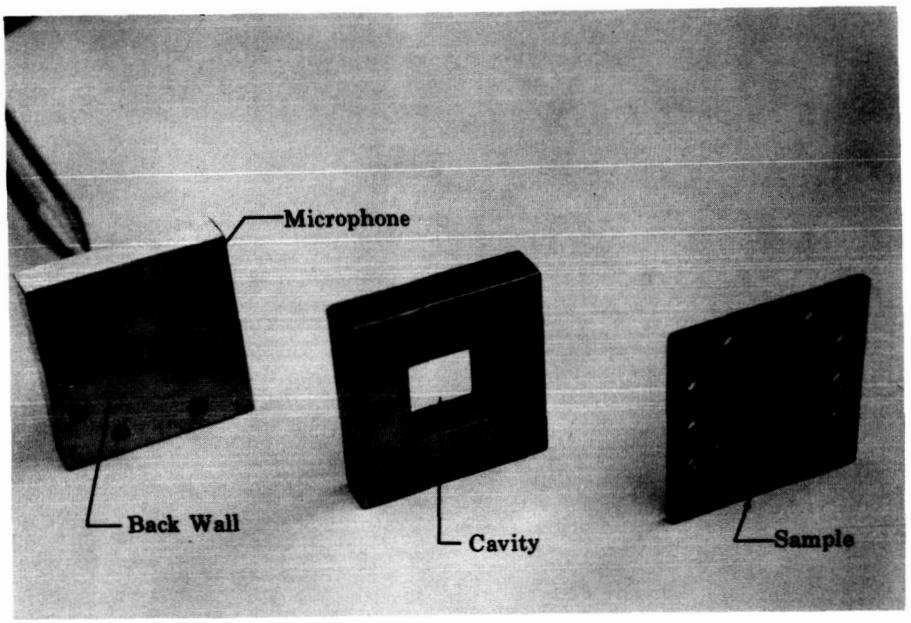

Figure VII-1. High Frequency Sound Wave Measuring Device FD 23078

C. ANALYSIS

A sample having an open area ratio of 5.4%, a thickness 0.10 in., and an aperture diameter of 0.052 in. was used in a series of tests made at frequency intervals of 100 Hz over a range from 700 to 5500 Hz. A backing cavity having a depth of 0.800 in. was used. The total sound pressure level in front of the sample was maintained at 151 db.

Figure VII-2 shows how the sound pressure level in the cavity changed as the frequency was increased; it is worthy of note that the cavity sound level reaches a maximum before resonance occurs. Also, when the

frequency was increased beyond resonance, the sound pressure in the cavity drops below the pressure incident on the sample. This phenomenon occurs because the velocity of the gases in the apertures decreases as the frequency increases, thereby causing the sound energy to be transmitted through the apertures with less efficiency. Similar results from earlier tests have been reported (Reference 9).

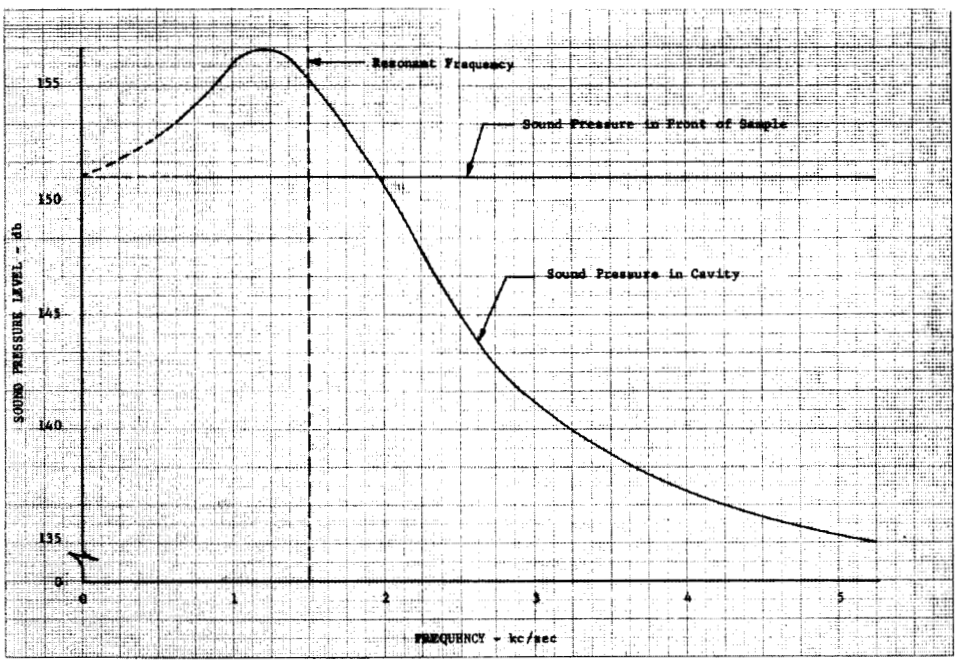

Figure VII-2. Cavity Sound Pressure Level vs Frequency DF 59729

The total sound pressure level in front of the sample was held constant at 151 db; however, the incident sound pressure varied with frequency, as seen in figure VII-3. Near resonance, the incident sound pressure level is almost equal to the total sound pressure level, a condition that occurs when the absorption coefficient is near unity. Figure VII-4 shows that the measured absorption coefficient was 99.8%, i.e., 99.8% of the incident sound energy was absorbed and only 0.2% reflected. As explained in the previous section, the disagreement between experimental and theoretical values at high frequencies is due to the extrapolation of nonlinear resistance data that are obtained at low frequencies into the high frequency range.

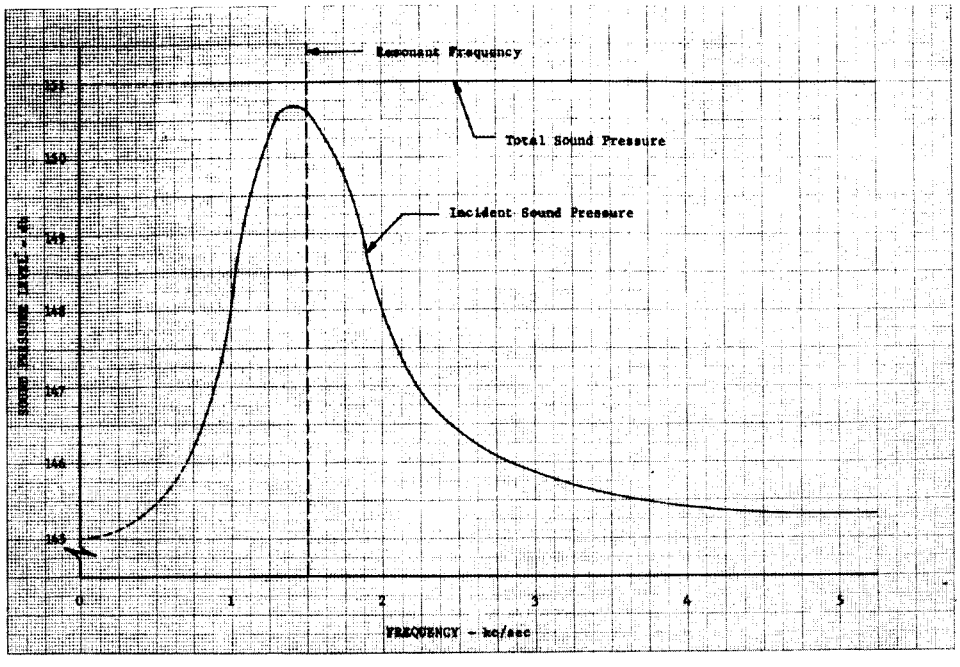

Figure VII-3. Incident Sound Pressure Level vs Frequency

DF 59730

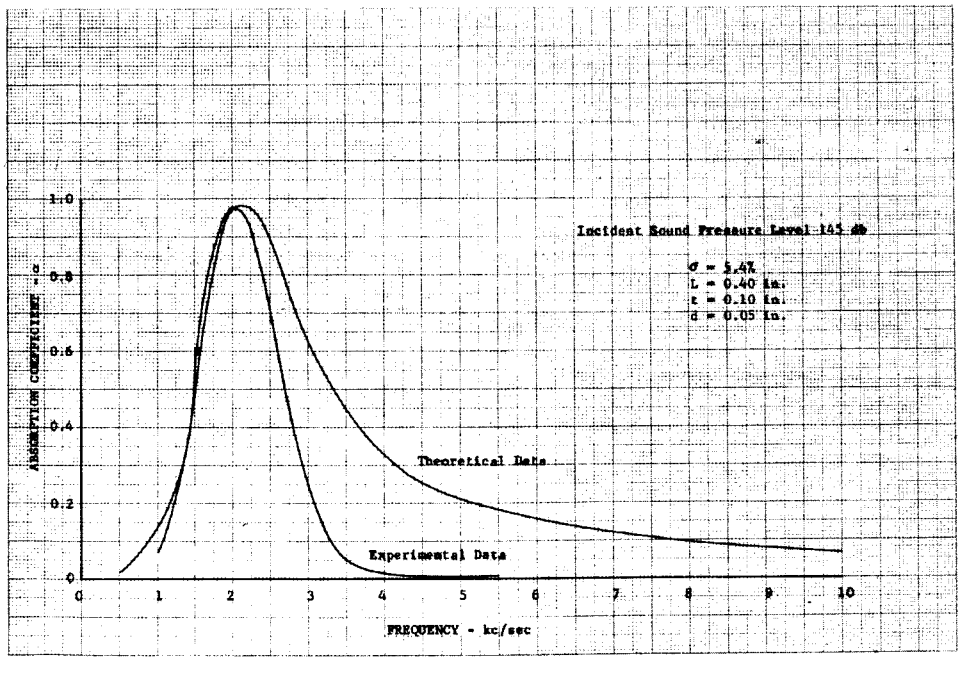

Figure VII-4. High Frequency Data Comparison

DF 59907

The specific acoustic reactance may be computed from:

$$X = \left[\frac{2\pi f_o \ell_{eff}}{c\sigma}\right]\left[\frac{f}{f_o} - \frac{f_o}{f}\right] \qquad \text{(VII-1)}$$

where $$f_o = \frac{c}{2\pi}\sqrt{\frac{\sigma}{L\,\ell_{eff}}} \qquad \text{(VII-2)}$$

and $$\ell_{eff} = t + 0.85\,d\,(1-0.7\sqrt{\sigma}) \qquad \text{(VII-3)}$$

For present purposes it is useful to combine equations (VII-8) and (VII-9) to obtain:

$$X = \frac{2\pi}{c}\left(\frac{\ell_{eff}}{\sigma}\right) f - \left(\frac{c}{2\pi}\right)\left(\frac{1}{L}\right)\left(\frac{1}{f}\right) \qquad \text{(VII-4)}$$

where the term containing ℓ_{eff} is the inertance and the term containing L is the capacitance. The acoustic resistance of an array of resonators can theoretically be predicted using the equations of Section III of this report.

To investigate the validity of the theory at high frequencies, the components of impedance were computed and compared with experimental data; the results are shown in figures VII-5 and VII-6. The capacitance of the array was found to agree with theory over the entire frequency range. Significant deviations between the theory and experimental data were noted for both the inertance and resistance, especially at frequencies greater than that of resonance. Further study of the data revealed that the discrepancies in the inertance and resistance components are due to inaccuracies in the effective length and nonlinear resistance correction factors. Both of these terms must be computed from empirical correlations of data. No impedance data on the performance of resonator arrays operating at high sound pressure levels in the high frequency regime (above 2000 Hz) were available when the empirical correlations were formed; therefore, it is not surprising to find that extrapolations into this regime produce inaccuracies. It is worthy of note that no empirical data are required for the computation of the theoretical capacitance term.

D. RECOMMENDATIONS

It is recommended that additional research be conducted in an attempt to improve the absorbing liner design techniques in the high frequency,

high sound pressure level regime. Until the theory can be improved, absorbing liners for operation at frequencies greater than 2000 Hz should be designed so that the resonant frequency of the assembly is greater than the frequency at which the instability occurs.

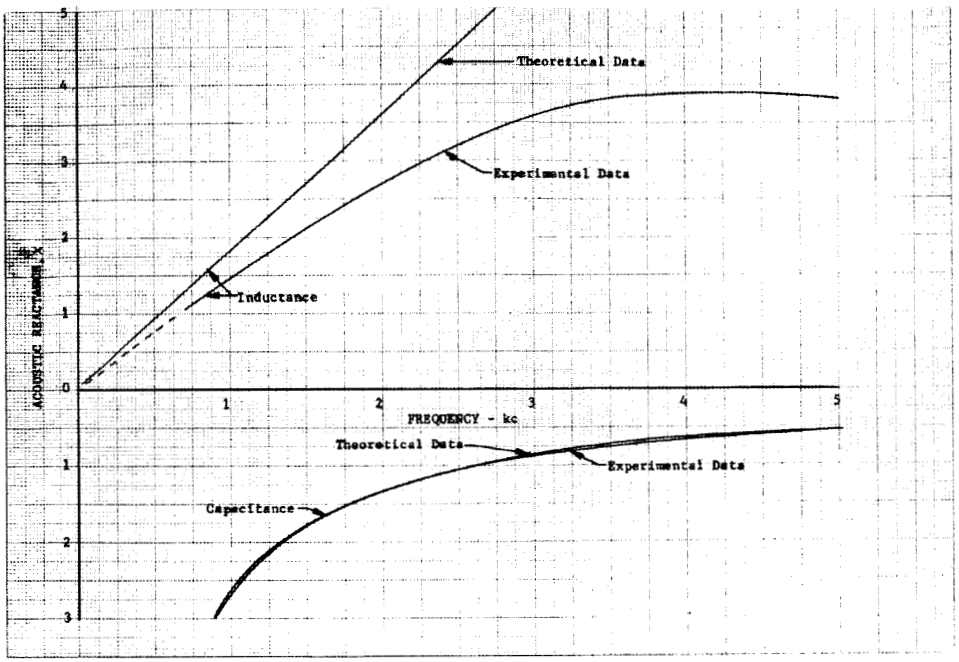

Figure VII-5. Comparison of Experimental Inertance and Capacitance With Theoretical DF 59702

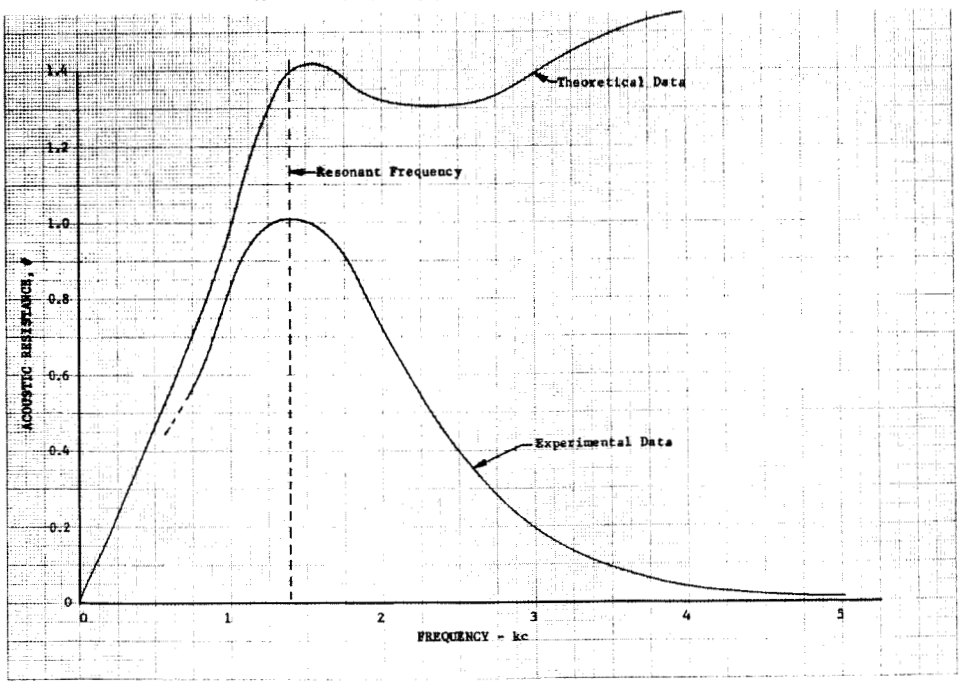

Figure VII-6. Comparison of Experimental Acoustic Resistance to Theoretical DF 59700

The phase angle technique has proven to be a precise and accurate method of measuring the acoustic characteristics of absorbers. A similar technique could possibly be used to measure the absorbing coefficient of a liner and the incident energy causing the instability in a rocket chamber under actual firing conditions. Such measurements could lead to significant improvements in the design theory; therefore, it is recommended that the feasibility and limitations of the technique for such applications be investigated further.

SECTION VIII
REFERENCES

1. "A Study of the Suppression of Combustion Oscillations With Mechanical Damping Devices," Summary Report of Tasks I and II, Pratt & Whitney Aircraft Report No. PWA FR-1007, 5 August 1964 (Confidential)

2. "A Study of the Suppression of Combustion Oscillations With Mechanical Damping Devices," Summary Report of Tasks III through VI, Pratt & Whitney Aircraft Report No. PWA FR-1115, 28 November 1964.

3. Ingard, U., "On the Theory and Design of Acoustic Resonators," JASA, Volume 25, No. 6, November 1953.

4. Blackman, A.W., "Effect of Nonlinear Losses on the Design of Absorbers for Combustion Instabilities," ARS Journal, November 1960, p 1022.

5. "Standard Method of Test for Impedance and Absorption of Acoustical Materials by the Tube Method," ASTM Designation: C 384-58, 1959.

6. "A Study of the Suppression of Combustion Oscillations With Mechanical Damping Devices," Phase II Summary Report, Pratt & Whitney Aircraft, FR-1922, 15 July 1966.

7. Dodge, Barnett F., Chemical Engineering Thermodynamics, McGraw-Hill Book Company, Inc., New York and London, 1944, p. 328.

8. Kinsler, L.E., and A.R. Frey, "Fundamentals of Acoustics," Second Edition, John Wiley and Sons, Inc., New York, New York, 1962, pp. 225 and 241.

9. Ingard, Uno, "The Near Field of a Helmholtz Resonator Exposed to a Plane Wave," JASA, Volume 25, No. 6, p 1066, November 1953.

10. Garrison, G. D., "Absorbing Liners for Rocket Combustion Chambers - Theory and Design Techniques," Pratt and Whitney Aircraft, AFRPL-TR-66-234, August 1966.

APPENDIX A
ANALYSIS OF SERIES RESONATOR

The single Helmholtz resonator or its electrical and mechanical equivalent is a dynamical system, whose motion is constrained so that its position can be completely specified by one coordinate. Vibrating systems of this type are said to have one degree of freedom. The double resonator configuration is a system of two elements that are capable of vibrating independently of each other. Therefore, the double resonator in series and its equivalent electric circuit (figure A-1) are harmonic oscillators whose motion has two degrees of freedom.

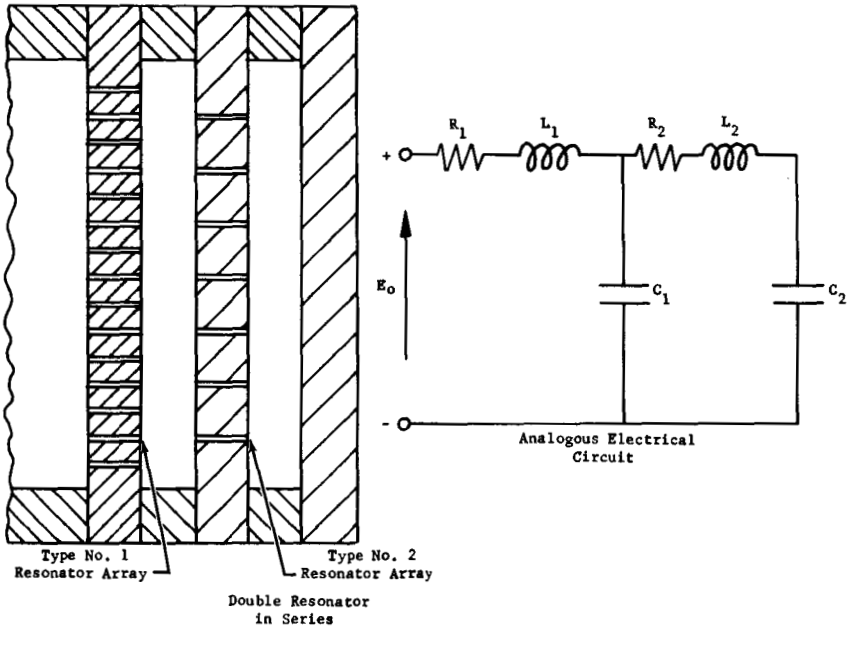

Figure A-1. Acoustic-Electric Analogy for Series Double Resonator FD 20215A

The equations of motion for oscillators with two degrees of freedom are given in many texts*. For our purposes, it is more convenient using the analogous electrical circuit to analyze the double resonator system. The impedance of the acoustical system can then be determined by (1) solving

---

* Jacobsen, L. S., and R. S. Ayre, Engineering Vibrations, p 317, McGraw-Hill Inc., New York, N.Y., 1958.

its equivalent electrical circuit and (2) substituting the acoustic elements of the system for their associated elements in the circuit.

The electrical analogue of the double resonator will be solved to determine the equivalent impedance. Acoustic absorption of the system can then be calculated from the final impedance results.

For convenience the following substitutions are made for the circuit given in figure A-1:

$$Z_1 = R_1 + i\left(X_{L_1}\right) \qquad \text{where: } i = \sqrt{-1}$$

$$Z_2 = i\left(X_{C_1}\right)$$

$$Z_3 = R_2 + i\left(X_{L_2} + X_{C_2}\right)$$

Total equivalent impedance can be expressed as follows:

$$Z_{eq} = Z_1 + \frac{Z_2 Z_3}{Z_2 + Z_3}$$

By substitution:

$$Z_{eq} = \left(R_1 + i\,X_{L_1}\right) + \frac{i\,X_{C_1}\left[R_2 + i\left(X_{L_2} + X_{C_2}\right)\right]}{i\,X_{C_1} + \left[R_2 + i\left(X_{L_2} + X_{C_2}\right)\right]}$$

$$Z_{eq} = \left[R_1 + \frac{X_{C_1}{}^2 R_2}{R_2{}^2 + \left(X_{C_1} + X_{C_2} + X_{L_2}\right)^2}\right] +$$

$$i\left[X_{L_1} + \frac{X_{C_1} R_2{}^2 + X_{C_1}{}^2\left(X_{C_2} + X_{L_2}\right) + X_{C_1}\left(X_{C_2} + X_{L_2}\right)^2}{R_2{}^2 + \left(X_{C_1} + X_{C_2} + X_{L_2}\right)^2}\right]$$

The equivalent impedance is now expressed by real and imaginary terms. Substituting for the reactive terms:

$$X_{L_1} = \omega L_1 \qquad X_{L_2} = \omega L_2$$

$$X_{C_1} = -\frac{1}{\omega C_1} \qquad X_{C_2} = -\frac{1}{\omega C_2}$$

where: ω = angular frequency (rad/sec)

$$\therefore \quad Z_{eq} = \left[R_1 + \frac{\left(\frac{1}{\omega C_1}\right)^2 R_2}{R_2^2 + \left(\omega L_2 - \frac{1}{\omega C_2} - \frac{1}{\omega C_1}\right)^2} \right] +$$

$$i \left[\omega L_1 + \frac{-\frac{1}{\omega C_1} R_2^2 + \left(\frac{1}{\omega C_1}\right)^2 \left(\omega L_2 - \frac{1}{\omega C_2}\right) - \frac{1}{\omega C_1}\left(\omega L_2 - \frac{1}{\omega C_2}\right)^2}{R_2^2 + \left(\omega L_2 - \frac{1}{\omega C_2} - \frac{1}{\omega C_1}\right)^2} \right]$$

The absorption coefficient is defined as the ratio of energy absorbed to energy of the incident pressure wave. In terms of specific acoustic impedance the absorption may be calculated from the following expression:

$$\alpha = 1 - \left| \frac{Z_{eq} - 1}{Z_{eq} + 1} \right|^2$$

Resonant frequency expressions for the double resonator in series may be determined by setting the imaginary component of equivalent impedance equal to zero. Results are not presented because the equations become too cumbersome for presentation purposes.

APPENDIX B
ANALYSIS OF PARALLEL RESONATOR

The double resonator in parallel is similar to the double resonator in series since both configurations are harmonic oscillators whose motion has two degrees of freedom. A double resonator in parallel and its equivalent electrical circuit are given in figure B-1.

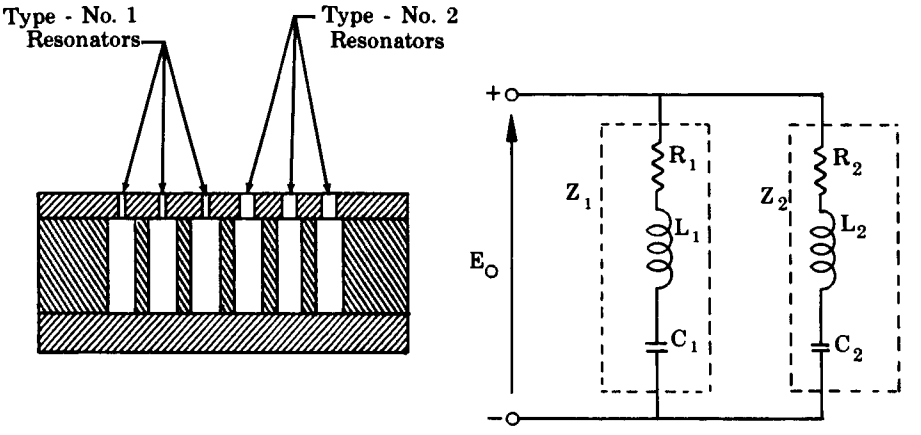

Figure B-1. Acoustic-Electric Analogy for Parallel Double Resonator FD 23079

The impedance of the acoustical system can be determined by (1) solving its equivalent electrical circuit and (2) by substituting the acoustic elements of the system for their associated elements in the circuit. The parallel resonator circuit will now be solved for the equivalent impedance term and the resulting absorption coefficient. A method for determining resonant frequency values is also presented.

Using the circuit of figure B-1 the component impedances are written as:

$$Z_1 = R_1 + i\left(X_{L_1} + X_{C_1}\right)$$

$$Z_2 = R_2 + i\left(X_{L_2} + X_{C_2}\right)$$

where: $i = \sqrt{-1}$

The total equivalent impedance can be expressed as follows:

$$Z_{eq} = \frac{Z_1 \; Z_2}{Z_1 + Z_2}$$

By substitution:

$$Z_{eq} = \frac{\left[R_1 + i\left(X_{L_1} + X_{C_1}\right)\right] + \left[R_2 + i\left(X_{L_2} + X_{C_2}\right)\right]}{\left[R_1 + i\left(X_{L_1} + X_{C_1}\right)\right] + \left[R_2 + i\left(X_{L_2} + X_{C_2}\right)\right]}$$

$$Z_{eq} = \left[\frac{\left[R_1R_2 - \left(X_{L_1} + X_{C_1}\right)\left(X_{L_2} + X_{C_2}\right)\right]\left(R_1 + R_2\right) + \left[R_1\left(X_{L_2} + X_{C_2}\right) + R_2\left(X_{L_1} + X_{C_1}\right)\left(X_{L_1} + X_{C_1} + X_{L_2} + X_{C_2}\right)\right]}{\left(R_1 + R_2\right)^2 + \left(X_{L_1} + X_{C_1} + X_{L_2} + X_{C_2}\right)^2}\right] +$$

$$i\left[\frac{\left[R_1\left(X_{L_2} + X_{C_2}\right) + R_2\left(X_{L_1} + X_{C_1}\right)\right]\left(R_1 + R_2\right) - \left[R_1R_2 - \left(X_{L_1} + X_{C_1}\right)\left(X_{L_2} + X_{C_2}\right)\right]\left(X_{L_1} + X_{C_1} + X_{L_2} + X_{C_2}\right)}{\left(R_1 + R_2\right)^2 + \left(X_{L_1} + X_{C_1} + X_{L_2} + X_{C_2}\right)^2}\right]$$

The equivalent impedance is now expressed in terms of real and imaginary components. Substituting for the reactive terms:

$$X_{L_1} = L_1 \qquad X_{L_2} = L_2$$

$$X_{C_1} = -\frac{1}{\omega C_1} \qquad X_{C_2} = -\frac{1}{\omega C_2}$$

where: ω = angular frequency (rad/sec)

$$Z_{eq} = \left[\frac{\left[R_1R_2 - \left(\omega L_1 - \frac{1}{\omega C_1}\right)\left(\omega L_2 - \frac{1}{\omega C_2}\right)\right]\left(R_1 + R_2\right) + \left[R_1\left(\omega L_2 - \frac{1}{\omega C_2}\right) + R_2\left(\omega L_1 - \frac{1}{\omega C_1}\right)\left(\omega L_1 - \frac{1}{\omega C_1} + \omega L_2 - \frac{1}{\omega C_2}\right)\right]}{\left(R_1 + R_2\right)^2 + \left(\omega L_1 - \frac{1}{\omega C_1} + \omega L_2 - \frac{1}{\omega C_2}\right)^2}\right] +$$

$$- i\left[\frac{\left[R_1\left(\omega L_2 - \frac{1}{\omega C_2}\right) + R_2\left(\omega L_1 - \frac{1}{\omega C_1}\right)\right]\left(R_1 + R_2\right) - \left[R_1R_2 - \left(\omega L_1 - \frac{1}{\omega C_1}\right)\left(\omega L_2 - \frac{1}{\omega C_2}\right)\right]\left(\omega L_1 - \frac{1}{\omega C_1} + \omega L_2 - \frac{1}{\omega C_2}\right)}{\left(R_1 + R_2\right)^2 + \left(\omega L_1 - \frac{1}{\omega C_1} + \omega L_2 - \frac{1}{\omega C_2}\right)^2}\right]$$

The absorption coefficient is defined as the ratio of energy absorbed to the energy of the incident pressure wave. In terms of the specific acoustic impedance the absorption coefficient can be calculated from:

$$\alpha = 1 - \left| \frac{Z_{eq} - 1}{Z_{eq} + 1} \right|^2$$

Expressions for the resonant frequencies may be calculated by setting the imaginary term of the equivalent impedance equal to zero. The terms become too cumbersome to establish resonant frequency equations in general terms so the results are not presented. By inspecting the experimental data in figure V-31, a method was derived for determining the two observed resonant frequencies of a parallel double resonator. The lower resonant frequency, f_{o1}, of the parallel configuration corresponds to the lower natural frequency of the individual types.

That is: $f_{o1} = f_{oa}$

where:

f_{o1} = first resonant frequency of parallel double resonator

f_{o2} = second resonant frequency of parallel double resonator

$f_{o1} < f_{o2}$

f_{oa} = resonant frequency of Type A resonator

f_{ob} = resonant frequency of Type B resonator

$f_{oa} < f_{ob}$

The higher of the resonant frequencies for the parallel contiguration, f_{o2}, may be calculated in the following manner:

For an array:

$$f_o = \frac{C}{2\pi} \sqrt{\frac{\sigma}{\ell_{eff\ L}}}$$

$$= \frac{C}{2\pi} \sqrt{\frac{A}{V\ell_{eff}}}$$

$$\therefore f_{o2} = \frac{C}{2\pi} \sqrt{\frac{A_t}{V_t (\ell_{eff})_{avg}}}$$

where:

A_t = total aperture area

V_t = total cavity volume

$(\ell_{eff})_{avg}$ = average calculated effective length

The above analysis applies only to the parallel double resonator with individual cavities. For an array type configuration with a common backing volume, only one resonant frequency would be observed and could be calculated using an average value for each term in the resonant frequency equation.

The shift of f_{o2} to a value lower than f_{ob} can be explained in terms of the incident sound pressure level. In an impedance tube test with a standard single-type-resonator configuration, the incident pressure wave is distributed evenly across the face of the resonant sample. A parallel double resonator produces distortion of the sound wave at the sample face because of the double impedances present. Due to this distortion the parallel configuration does not have a performance equivalent to that of two different resonators performing separately. It should be remembered that the solution of the parallel double resonator circuit is based on an undistorted incidence pressure wave. As a result, analytical equations from the circuit analogy will not produce results that are exactly equivalent to experimental data.

APPENDIX C
DERIVATION OF IMPEDANCE EQUATION

A typical Helmholtz resonator at the end of a tube is shown in the figure below:

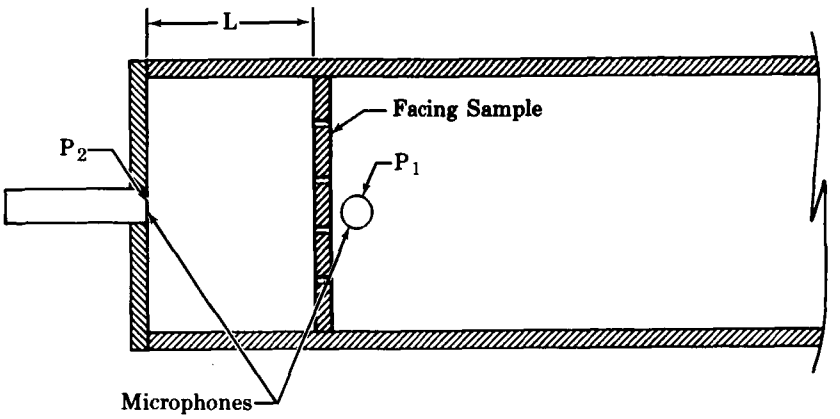

Figure C-1. Helmholtz Resonator in Impedance Tube FD 23080

Shown in the figure are two microphones, one mounted in the side wall to measure the sound pressure in front of the sample and one on the rear wall of the cavity. With the signals from both microphones the phase difference between the two pressure waves can be determined.

The total impedance at the end of the tube is

$$Z_{total} = Z_{plate} + Z_{air\ cavity} \tag{C-1}$$

where by definition

$$Z_{plate} = \frac{P_1 - P_2}{\psi u} \tag{C-2}$$

and also

$$Z_{air\ cavity} = \frac{P_2}{\psi u} = \frac{i}{kL} \tag{C-3}$$

Solving C-2 for u, substituting into C-3 and solving for Z_{plate} gives:

$$Z_{plate} = \frac{i}{kL}\left[\frac{P_1}{P_2} - 1\right] \tag{C-4}$$

Using a mathematical identity, the ratio of complex pressures can be expressed as:

$$\frac{P_1}{P_2} = \left|\frac{P_1}{P_2}\right| e^{-i\phi} = \left|\frac{P_1}{P_2}\right| \cos\phi - i\left|\frac{P_1}{P_2}\right| \sin\phi$$

Substituting the identity into C-4 gives:

$$Z_{plate} = \frac{i}{kL}\left|\frac{P_1}{P_2}\right| \sin\phi - \frac{i}{kL}\left[1 - \left|\frac{P_1}{P_2}\right| \cos\phi\right]$$

Solving C-1 for Z_{total} gives:

$$Z_{total} = \frac{1}{kL}\left|\frac{P_1}{P_2}\right| \sin\phi - \frac{i}{kL}\left[1 - \left|\frac{P_1}{P_2}\right| \cos\phi\right] + \frac{i}{kL} \qquad \text{(C-5)}$$

$$Z_{total} = \frac{1}{kL}\left|\frac{P_1}{P_2}\right| \sin\phi + i\left[\frac{1}{kL}\left|\frac{P_1}{P_2}\right| \cos\phi\right] \qquad \text{(C-6)}$$

From C-6 the acoustic resistance is:

$$\theta = \frac{1}{kL}\left|\frac{P_1}{P_2}\right| \sin\phi$$

Also the acoustic reactance is:

$$X = -\frac{1}{kL}\left|\frac{P_1}{P_2}\right| \cos\phi$$

APPENDIX D
DERIVATION OF THE INCIDENT SPL EQUATION

When a longitudinal sound wave is incident on an array of resonators, part of the incident sound intensity (I_i) is transmitted (I_t) and the remaining part is reflected (I_r) as shown in the following sketch:

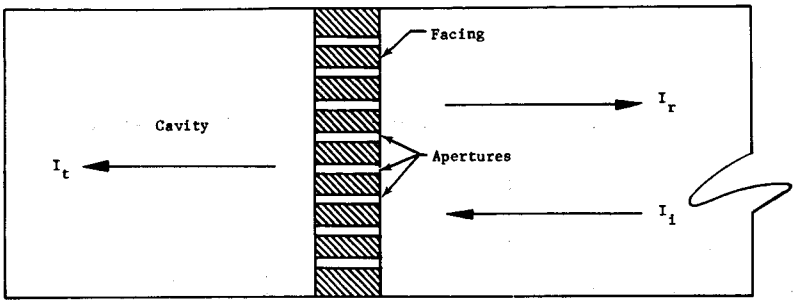

The transmitted wave may be represented by:

$$I_t = I_i - I_r \tag{D-1}$$

The intensity can be written as $I = P^2/2\rho c$; therefore equation (D-1) can be written as

$$P_t^2 = P_i^2 - P_r^2 \tag{D-2}$$

The absorption coefficient is given by

$$\alpha = \frac{I_t}{I_i} = \left[\frac{P_t}{P_i}\right]^2 \tag{D-3}$$

Substituting equation (D-2) into (D-3) and simplifying gives

$$\alpha = 1 - \left[\frac{P_r}{P_i}\right]^2 \tag{D-4}$$

Absorption is defined by the following equation

$$\alpha = 1 - \left[\frac{Z - 1}{Z + 1}\right]^2 \tag{D-5}$$

where Z is the impedance of the resonator array.

Setting equations (D-4) and (D-5) equal,

$$\frac{P_r}{P_i} = \frac{Z - 1}{Z + 1} \tag{D-6}$$

The total sound pressure (P_1) is given by

$$P_1 = P_i + P_r \tag{D-7}$$

Solving equation (D-7) for P_r and substituting into equation (D-6) gives

$$\frac{P_1 - P_i}{P_i} = \frac{Z - 1}{Z + 1} \tag{D-8}$$

Simplifying and solving for the total sound pressure gives

$$P_1 = P_i \left[1 + \frac{Z - 1}{Z + 1} \right] \tag{D-9}$$

When the system in question is an array of Helmholtz resonators, simplifying equation (D-9) will give

$$P_1 = \frac{2Z_{tot}}{Z_{tot} + 1} P_i \tag{D-10}$$

where the total impedance of the resonator is defined as

$$Z_{tot} = Z_{plate} + Z_{air\ cavity} \tag{D-11}$$

and

$$Z_{plate} = (\theta - iX_p) \tag{D-12}$$

and

$$Z_{air\ cavity} = \frac{i}{kL} \tag{D-13}$$

Using these definitions and substituting into equation (D-10) gives

$$P_1 = \frac{2\left(\theta - iX_p + \frac{i}{kL}\right)}{(\theta + 1) - i\left(X_p - \frac{i}{kL}\right)} P_i \tag{D-14}$$

or

$$P_1 = \frac{2\left[\theta^2 + \left(X_p - \frac{1}{kL}\right)^2\right]^{1/2}}{\left[(\theta + 1)^2 + \left(X_p - \frac{1}{kL}\right)^2\right]^{1/2}} P_i \qquad \text{(D-15)}$$

The incident sound pressure can be solved from equation (D-16) after the resistance and reactance of the resonator are determined from the technique given in Section VI.

$$P_i = P_1 \frac{\left[(\theta + 1)^2 + X^2\right]^{1/2}}{2\left[\theta^2 + X^2\right]^{1/2}} \qquad \text{(D-16)}$$

where

$$X = X_p - \frac{1}{kL}$$

APPENDIX E
DISTRIBUTION LIST

The report is to be sent directly to the recipient except where the technical librarian for the recipient is designated. In these cases the report is to be sent to the librarian and a copy of the transmittal letter to the recipient.

NASA Headquarters 2
Washington D.C. 20546
Attn: Dr. R. S. Levine, RPL

NASA Headquarters 2
Washington D.C. 2054o
Attn: Mr. A. O. Tischler, RP

NASA Headquarters 2
Washington D.C. 20546
Attn: Mr. Edward Z. Gray, Director
Advanced Manned Missions, MT
Office of Manned Space Flight

NASA Marshall Space Flig 6
Center
Huntsville, Alabama 35812
Attn: Purchasing Office, PR-SC

NASA Marshall Space Flight 1
Center
Huntsville, Alabama 35812
Attn: Scientific and Technical
Information Branch, MS-IP

NASA Marshall Space Flight 1
Center
Huntsville, Alabama 35812
Attn: Patent Office, CC-P

NASA Marshall Space Flight 1
Center
Huntsville, Alabama 35812
Attn: Technology Utilization
Office, MS-T

NASA Marshall Space Flight 1
Center
Huntsville, Alabama 35812
Attn: Mr. Robert Richmond,
R-P&VE-PAB

NASA Marshall Space Flight 3
Center
Huntsville, Alabama 35812
Attn: Mr. Rex Bailey,
R-P&VE-PAA

NASA Marshall Space Flight 1
Center
Huntsville, Alabama 35812
Attn: Mr. Keith Chandler,
R-P&VE-PA

NASA Ames Research Center 1
Moffett Field, California 94035
Attn: Technical Librarian for
Dr. H. J. Allen, Director

NASA Goddard Space Flight 1
Center
Greenbelt, Maryland 20771
Attn: Technical Librarian for
Merland L. Moseson, Code 620

NASA Lewis Research Center 1
21000 Brookpark Road
Cleveland, Ohio 44135
Attn: Dr. Richard Priem

NASA Lewis Research Center 2
21000 Brookpark Road
Cleveland, Ohio 44135
Attn: Mr. E. W. Conrad

NASA Lewis Research Center 1
21000 Brookpark Road
Cleveland, Ohio 44135
Attn: Technical Librarian for
Dr. Abe Silverstein,
Director

NASA Jet Propulsion Laboratory
California Institute of Technology
4800 Oak Grove Drive
Pasadena, California 91103
Attn: Technical Librarian for Robert F. Rose, Propulsion Division, 38
1

NASA Jet Propulsion Laboratory
California Institute of Technology
4800 Oak Grove Drive
Pasadena, California 91103
Attn: Mr. Jack H. Rupe
1

NASA Langley Research Center
Langley Station
Hampton, Virginia 23365
Attn: Technical Librarian for Floyd L. Thompson, Director
1

NASA Manned Spacecraft Center
Houston, Texas 77001
Attn: Technical Librarian for Robert R. Gilruth, Director
1

NASA Manned Spacecraft Center
Houston, Texas 77001
Attn: Mr. J. G. Thibodaux, EP
1

NASA John F. Kennedy Space Center
Cocoa Beach, Florida 32931
Attn: Technical Librarian for Dr. Kurt H. Debus, Director
1

Scientific and Technical Information Facility
P.O. Box 33
College Park, Maryland 20740
24

Advanced Research Projects Agency
Washington 25, D.C.
Attn: Technical Librarian for Dr. D. E. Mock
1

Defense Documentation Center
Headquarters
Cameron Station, Bldg. 5
5010 Duke Street
Alexandria, Virginia 22314
Attn: Technical Librarian for TISIA
1

Picatinny Arsenal
Dover, New Jersey 07801
Attn: Technical Librarian for Mr. I. Forsten, Chief, Liquid Propulsion Laboratory, SMUPA-DL
1

Rocket Research Laboratories
Edwards Air Force Base
Edwards, California 93523
Attn: Technical Librarian
1

Rocket Research Laboratories
Edwards Air Force Base
Edwards, California 93523
Attn: Mr. Richard R. Weiss, RPRR
1

U.S. Army Missile Command
Redstone Arsenal, Alabama 35809
Attn: Technical Librarian for Gen. Zierdt
1

U.S. Army Missile Command
Redstone Arsenal, Alabama 35809
Attn: Dr. Walter W. Wharton, AMSMI-RRK
1

U.S. Naval Ordnance Test Station
China Lake, California 93557
Attn: Technical Librarian for Chief, Missile Propulsion Division, Code 4562
1

U.S. Naval Ordnance Test Station
China Lake, California 93557
Attn: Mr. Edward W. Price, Code 5008
1

Chemical Propulsion Information Agency
Johns Hopkins University
Applied Physics Laboratory
8621 Georgia Avenue
Silver Spring, Maryland 20910
Attn: Technical Librarian for Tom Reedy
1

Chemical Propulsion Information Agency
Johns Hopkins University
Applied Physics Laboratory
8621 Georgia Avenue
Silver Spring, Maryland 20910
Attn: Mr. T.W. Christian — 1

ARL
Wright-Patterson AFB
Dayton, Ohio 45433
Attn: Mr. K. Scheller, Bldg. 450 — 1

Headquarters
Air Force Office of Scientific Research
Propulsion Division
Washington, D.C.
Attn: Dr. Bernard T. Wolfson — 1

Department of the Navy
Office of Naval Research
Washington, D.C. 20360
Attn: Mr. R. O. Jackel — 1

RTNT
Bolling Field
Washington, D.C. 20332
Attn: Dr. L. Green, Jr. — 1

Aerojet-General Corporation
P.O. Box 1947
Sacramento, California 95809
Attn: Technical Librarian for Mr. R. Stiff — 1

Aerojet-General Corporation
P.O. Box 1947
Sacramento, California 95809
Attn: Dr. Robert J. Hefner — 1

Aerospace Corporation
P.O. Box 95085
Los Angeles, California 90045
Attn: Technical Librarian for Mr. J. C. Wilder — 1

Aerospace Corporation
P.O. Box 95085
Los Angeles, California 90045
Attn: Mr. O. W. Dykema — 1

Aerospace Corporation
P.O. Box 95085
Los Angeles, California 90045
Attn: Dr. W. G. Strahle — 1

Arther D. Little, Inc.
Acorn Park
Cambridge, Massachusetts 02140
Attn: Technical Librarian for Dr. E. K. Bastress — 1

Bell Aerosystems Company
P.O. Box 1
Buffalo 5, New York
Attn: Technical Librarian for Mr. W. M. Smith — 1

Bell Aerosystems Company
P.O. Box 1
Buffalo 5, New York
Attn: Dr. Theodor G. Rossmann — 1

Boeing Company
P.O. Box 3707
Seattle, Washington 98124
Attn: Technical Librarian for Mr. J. D. Alexander — 1

Curtiss-Wright Corporation
Wright Aeronautical Division
Wood-ridge, New Jersey 07075
Attn: Technical Librarian for Mr. G. Kelly — 1

General Electric Company
Cincinnati, Ohio 45215
Attn: Technical Librarian for Mr. D. Suichu — 1

Lockheed Missiles and Space Company
Technical Information Center
P.O. Box 504
Sunnyvale, California 94088
Attn: Technical Librarian for Dr. Y.C. Lee — 1

The Marquardt Corporation
16555 Saticoy Street
Van Nuys, California 91409
Attn: Technical Librarian for Mr. Warren P. Boardman, Jr. — 1

North American Aviation, Inc. 1
Space and Information Systems Division
12214 Lakewood Boulevard
Downey, California
Attn: Technical Librarian for
Mr. H. Storms

Reaction Motors Division 1
Thiokol Chemical Corporation
Denville, New Jersey 07832
Attn: Technical Librarian for
Mr. Arthur Sherman

Reaction Motors Division 1
Thiokol Chemical Corporation
Denville, New Jersey 07832
Attn: Mr. O. Mann

Space Technology Laboratories 1
TRW Incorporated
One Space Park
Redondo Beach, California 90278
Attn: Mr. G. W. Elverum

Stanford Research Institute 1
333 Ravenswood Avenue
Menlo Park, California 94025
Attn: Technical Librarian for
Dr. Lionel Dickinson

Dynamic Science Corporation 1
1445 Huntington Drive
South Pasadena, California
Attn: Technical Librarian

TAPCO Division 1
TRW, Incorporated
23555 Euclid Avenue
Cleveland, Ohio 44117
Attn: Technical Librarian for
Mr. P. T. Angell

Thiokol Chemical Corporation 1
Redstone Division
Huntsville, Alabama
Attn: Technical Librarian for
Mr. John Goodloe

United Aircraft Corporation 1
South Administration Bldg. No. 2
400 Main Street
East Hartford, Connecticut 06108
Attn: Technical Librarian for
Mr. Erle Martin

United Aircraft Corporation 1
Research Laboratories 1
400 Main Street
East Hartford, Connecticut 06108
Attn: Mr. D. H. Utvik

United Technology Center 1
587 Mathilda Avenue 1
P.O. Box 358
Sunnyvale, California 94088
Attn: Technical Librarian for
Mr. B. Adelman

United Technology Center 1
587 Mathilda Avenue
P.O. Box 358
Sunnyvale, California 94088
Attn: Mr. R. H. Osborn

Rocketdyne Division of North 1
American Aviation
6633 Canoga Avenue
Canoga Park, California 91304
Attn: Technical Librarian for 1
Mr. S. Hoffman

Rocketdyne Division of North 1
American Aviation
6633 Canoga Avenue
Canoga Park, California 91304 1
Attn: Dr. Robert B. Lawhead

Rocketdyne Division of North 1
American Aviation
6633 Canoga Avenue
Canoga Park, California 91304
Attn: Mr. Eugene Clinger 1

Warner-Swasey Company 1
Control Instrument Division
32-16 Downing Street
Flushing, New York 11354
Attn: Mr. R. H. Tourin

Rocket Research Corporation
520 South Portland Street
Seattle, Washington 98108
Attn: Technical Librarian for
Mr. Robert Bridgeforth — 1

Defense Research Corporation
P.O. Box 3587
Santa Barbara, California
Attn: Mr. B. Gray — 1

Multi-Tech Inc.
Box 4186 No. Annex
San Fernando, California
Attn: Mr. F. B. Cramer — 1

Geophysics Corporation of America
Technical Division
Bedford, Massachusetts
Attn: Mr. A. C. Tobey — 1

Polytechnic Institute of Brooklyn
Graduate Center
Route 110
Farmingdale, New York
Attn: Dr. V. D. Agosta — 1

Applied Physics Laboratory
The Johns Hopkins University
8621 Georgia Avenue
Silver Spring, Maryland 20910
Attn: Dr. W. G. Berl — 1

Ohio State University
Rocket Research Laboratory
Department of Aeronautical and Astronautical Engineering
Columbus 10, Ohio — 1

Princeton University
Forrestal Research Center
Princeton, New Jersey
Attn: Dr. I. Glassman — 1

Princeton University
Forrestal Research Center
Princeton, New Jersey
Attn: Mr. D. T. Harrje — 2

University of Wisconsin
Department Mechanical Engineering
1513 University Avenue
Madison, Wisconsin 53705
Attn: Dr. P. S. Myers — 1

Dartmouth University
Hanover, New Hampshire
Attn: Dr. P. D. McCormack — 1

University of Michigan
Aeronautical and Astronautical Engineering Laboratories
Aircraft Propulsion Lab.
North Campus
Ann Arbor, Michigan
Attn: Dr. J. A. Nicholls — 1

Institute of Engineering Research
University of California
Berkeley, California
Attn: Dr. A. K. Oppenheim — 1

Purdue University
School of Mechanical Engineering
Lafayette, Indiana
Attn: Dr. J. R. Osborn — 1

Massachusetts Institute of Technology
Department of Mechanical Engineering
Cambridge 39, Massachusetts
Attn: Dr. T. Y. Toong — 1

Illinois Institute of Technology
10 W. 35th Street
Chicago, Illinois
Attn: Dr. P. T. Torda — 1

Georgia Institute of Technology
Aerospace School
Atlanta, Georgia
Attn: Dr. Ben T. Zinn — 1